SANDIA REPORT

SAND2009-1127
Unlimited Release
Printed March 2009

Algorithmic Properties of the Midpoint Predictor-Corrector Time Integrator

E. Love
G. Scovazzi
W. J. Rider

Prepared by
Sandia National Laboratories
Albuquerque, New Mexico 87185 and Livermore, California 94550

Sandia is a multiprogram laboratory operated by Sandia Corporation,
a Lockheed Martin Company, for the United States Department of Energy's
National Nuclear Security Administration under Contract DE-AC04-94-AL85000.

Issued by Sandia National Laboratories, operated for the United States Department of Energy by Sandia Corporation.

Available to DOE and DOE contractors from
U.S. Department of Energy
Office of Scientific and Technical Information
P.O. Box 62
Oak Ridge, TN 37831

Telephone: (865) 576-8401
Facsimile: (865) 576-5728
E-Mail: reports@adonis.osti.gov
Online ordering: http://www.doe.gov/bridge

Available to the public from
U.S. Department of Commerce
National Technical Information Service
5285 Port Royal Rd
Springfield, VA 22161

Telephone: (800) 553-6847
Facsimile: (703) 605-6900
E-Mail: orders@ntis.fedworld.gov
Online ordering: http://www.ntis.gov/ordering.htm

SAND2009-1127
Unlimited Release
Printed March 2009

Algorithmic Properties of the Midpoint Predictor-Corrector Time Integrator

E. Love, G. Scovazzi and W. J. Rider
Computational Shock & MultiPhysics Department
MS-1319
Sandia National Laboratories
P.O. Box 5800
Albuquerque, NM 87185-1319

Abstract

Algorithmic properties of the midpoint predictor-corrector time integration algorithm are examined. In the case of a finite number of iterations, the errors in angular momentum conservation and incremental objectivity are controlled by the number of iterations performed. Exact angular momentum conservation and exact incremental objectivity are achieved in the limit of an infinite number of iterations. A complete stability and dispersion analysis of the linearized algorithm is detailed. The main observation is that stability depends critically on the number of iterations performed.

Contents

Algorithmic Properties of the Midpoint Predictor-Corrector Time Integrator

1 Introduction

This paper presents an analysis of the algorithmic properties of a midpoint predictor-corrector time integrator for Lagrangian shock hydrodynamics [32, 33]. In particular, the conservation and stability properties of the algorithm are detailed. The first two sections of the paper are focused on the conservation properties. It is shown that exact angular momentum conservation and exact incremental objectivity are achieved in the converged limit of an infinite number of iterations. In the case of a finite number of iterations, the errors are limited by the number of iterations performed. The remaining sections of the paper present a complete stability and dispersion analysis of the linearized algorithm. The authors have discovered that the algorithm does not yield stable solutions in the case of an odd number of iterations. An even number of iterations produces stable results. Numerical examples are provided to confirm the theoretical results. Included also are brief discussions of the time-stepping algorithms currently used in many codes [16, 25, 37, 40].

2 Angular Momentum

In the absence of applied external loading, the midpoint predictor-corrector time integration algorithm [32, 33] can be written in Lagrangian weak form as

$$\left.\begin{aligned} \int_{\Omega_0} \delta\boldsymbol{\varphi} \bullet \rho_0(\mathbf{v}_{n+1}^{(i+1)} - \mathbf{v}_n)\,\mathrm{d}\Omega_0 \;+\; \Delta\mathrm{t}\int_{\Omega_0} \mathrm{GRAD}[\delta\boldsymbol{\varphi}] \bullet \mathbf{F}_{n+1/2}^{(i)}\mathbf{S}_{n+1/2}^{(i)}\,\mathrm{d}\Omega_0 \;&=\; 0 \\ \boldsymbol{\varphi}_{n+1}^{(i+1)} - \boldsymbol{\varphi}_n - \Delta\mathrm{t}\cdot\mathbf{v}_{n+1/2}^{(i+1)} \;&=\; \mathbf{0} \end{aligned}\right\} \;\forall\, \delta\boldsymbol{\varphi}, \tag{1}$$

with time step $\Delta\mathrm{t} \geqslant 0$, where the index n corresponds to the time step index and the index (i) corresponds to the fixed-point iteration index. In the above, $\Omega_0 \subset \mathbb{R}^3$ is the fixed material domain, $\rho_0 > 0$ is the fixed material density, $\boldsymbol{\varphi} \in H^1(\Omega_0, \mathbb{R}^3)$ is the spatial coordinate, $\mathbf{v} \in H^1(\Omega_0, \mathbb{R}^3)$ is the spatial velocity, $\mathrm{GRAD}[\cdot] : H^1(\Omega_0, \mathbb{R}^3) \to L^2(\Omega_0, \mathbb{R}^3 \times \mathbb{R}^3)$ is the material gradient operator, $\mathbf{F} = \mathrm{GRAD}[\boldsymbol{\varphi}] \in L^2(\Omega_0, \mathbb{R}^3 \times \mathbb{R}^3)$ is the deformation gradient and $\mathbf{S} \in L^2(\Omega_0, \mathbb{R}^3 \times \mathbb{R}^3)$ is the *symmetric* second Piola-Kirchhoff stress. The algorithm is implemented in a staggered fashion. First, the velocity at time t_{n+1} is computed explicitly. Subsequently, the position $\boldsymbol{\varphi}_{n+1}$ is updated. To ensure second-order accuracy this iterative process is repeated at least two times.

Remarks 2.1. For a pressure-volume equation-of-state material model such as that used in [32, 33], the algorithmic stress $\mathbf{S}$ is defined by the relation

$$\left.\begin{aligned} J_{n+1/2}^{(i)}\, p_{n+1/2}^{(i)}\mathbf{I} \;&=\; \mathbf{F}_{n+1/2}^{(i)}\mathbf{S}_{n+1/2}^{(i)}\mathbf{F}_{n+1/2}^{(i)T} \\ p_{n+1/2}^{(i)} \;&=\; \frac{1}{2}\left(p_n + p_{n+1}^{(i)}\right) \end{aligned}\right\}, \tag{2}$$

where $p > 0$ is the thermodynamic pressure and $J := \det \mathbf{F}$. The stress $\mathbf{S}$ may also include contributions from artificial shock-capturing and hourglass-control viscosities. However, for developments here the only relevant consideration is that $\mathbf{S}$ remain symmetric.

Under suitable boundary conditions (pure Neumann), an admissible choice for $\delta\boldsymbol{\varphi}$ is $\delta\boldsymbol{\varphi} = \boldsymbol{\xi} \times \boldsymbol{\varphi}_{n+1/2}^{(j)}$, for some

$\boldsymbol{\xi} \in \mathbb{R}^3$ and using the midpoint position at iteration (j). This yields

$$\left.\begin{aligned} 0 &= \int_{\Omega_0} \boldsymbol{\xi} \times \boldsymbol{\varphi}^{(j)}_{n+1/2} \bullet \rho_0(\mathbf{v}^{(i+1)}_{n+1} - \mathbf{v}_n)\,\mathrm{d}\Omega_0 \;+\; \Delta\mathrm{t} \int_{\Omega_0} \mathrm{GRAD}[\boldsymbol{\xi} \times \boldsymbol{\varphi}^{(j)}_{n+1/2}] \bullet \mathbf{F}^{(i)}_{n+1/2}\mathbf{S}^{(i)}_{n+1/2}\,\mathrm{d}\Omega_0 \\ &= \int_{\Omega_0} \boldsymbol{\xi} \times \boldsymbol{\varphi}^{(j)}_{n+1/2} \bullet \rho_0(\mathbf{v}^{(i+1)}_{n+1} - \mathbf{v}_n)\,\mathrm{d}\Omega_0 \;+\; \Delta\mathrm{t} \int_{\Omega_0} \hat{\boldsymbol{\xi}}\mathbf{F}^{(j)}_{n+1/2} \bullet \mathbf{F}^{(i)}_{n+1/2}\mathbf{S}^{(i)}_{n+1/2}\,\mathrm{d}\Omega_0 \\ &= \int_{\Omega_0} \boldsymbol{\xi} \times \boldsymbol{\varphi}^{(j)}_{n+1/2} \bullet \rho_0(\mathbf{v}^{(i+1)}_{n+1} - \mathbf{v}_n)\,\mathrm{d}\Omega_0 \;+\; \Delta\mathrm{t} \int_{\Omega_0} \hat{\boldsymbol{\xi}} \bullet \mathbf{F}^{(i)}_{n+1/2}\mathbf{S}^{(i)}_{n+1/2}\mathbf{F}^{(j)T}_{n+1/2}\,\mathrm{d}\Omega_0 \\ &= \boldsymbol{\xi} \bullet \int_{\Omega_0} \boldsymbol{\varphi}^{(j)}_{n+1/2} \times \rho_0(\mathbf{v}^{(i+1)}_{n+1} - \mathbf{v}_n)\,\mathrm{d}\Omega_0 \;+\; \hat{\boldsymbol{\xi}}\Delta\mathrm{t} \bullet \int_{\Omega_0} \mathbf{F}^{(i)}_{n+1/2}\mathbf{S}^{(i)}_{n+1/2}\mathbf{F}^{(j)T}_{n+1/2}\,\mathrm{d}\Omega_0 \end{aligned}\right\}, \tag{3}$$

where $\hat{\boldsymbol{\xi}} \in \mathbb{R}^3 \times \mathbb{R}^3$ is the *skew-symmetric* tensor such that $\hat{\boldsymbol{\xi}}\mathbf{a} = (\boldsymbol{\xi} \times \mathbf{a})\ \forall \mathbf{a} \in \mathbb{R}^3$.

2.1 A Conserved Angular Momentum Quantity

A possible choice for (j) is $(j) = (i)$. This produces the conservation statement

$$\boldsymbol{\xi} \bullet \int_{\Omega_0} \boldsymbol{\varphi}^{(i)}_{n+1/2} \times \rho_0(\mathbf{v}^{(i+1)}_{n+1} - \mathbf{v}_n)\,\mathrm{d}\Omega_0 \;+\; \hat{\boldsymbol{\xi}}\Delta\mathrm{t} \bullet \int_{\Omega_0} \mathbf{F}^{(i)}_{n+1/2}\mathbf{S}^{(i)}_{n+1/2}\mathbf{F}^{(i)T}_{n+1/2}\,\mathrm{d}\Omega_0 \;=\; 0. \tag{4}$$

Notice however that

$$\underbrace{\hat{\boldsymbol{\xi}}}_{\text{skew-symmetric}} \quad \bullet \quad \underbrace{\mathbf{F}^{(i)}_{n+1/2}\mathbf{S}^{(i)}_{n+1/2}\mathbf{F}^{(i)T}_{n+1/2}}_{\text{symmetric}} \;=\; 0\,, \tag{5}$$

yielding the final conservation statement (since $\boldsymbol{\xi}$ is arbitrary)

$$\boxed{\int_{\Omega_0} \boldsymbol{\varphi}^{(i)}_{n+1/2} \times \rho_0(\mathbf{v}^{(i+1)}_{n+1} - \mathbf{v}_n)\,\mathrm{d}\Omega_0 \;=\; \mathbf{0}\,.} \tag{6}$$

Remarks 2.2. The total angular momentum defined as

$$\left.\begin{aligned} \mathsf{J}^{(i+1)}_{n+1} &:= \mathsf{J}_0 \;+\; \sum_{k=0}^{n} \left[\int_{\Omega_0} \boldsymbol{\varphi}^{(i)}_{k+1/2} \times \rho_0(\mathbf{v}^{(i+1)}_{k+1} - \mathbf{v}_k)\,\mathrm{d}\Omega_0\right] \\ \mathsf{J}_0 &:= \int_{\Omega_0} \boldsymbol{\varphi}_0 \times \rho_0\mathbf{v}_0\,\mathrm{d}\Omega_0 \end{aligned}\right\}, \tag{7}$$

is an exactly conserved quantity.

2.2 Non-Conserved Angular Momentum

Another choice for (j) is $(j) = (i+1)$. The first term on the right hand side of (3), after some algebraic manipulations, yields [35]

$$\boldsymbol{\xi} \bullet \int_{\Omega_0} \boldsymbol{\varphi}^{(i+1)}_{n+1/2} \times \rho_0(\mathbf{v}^{(i+1)}_{n+1} - \mathbf{v}_n)\,\mathrm{d}\Omega_0 = \boldsymbol{\xi} \bullet \left(\tilde{\mathsf{J}}^{(i+1)}_{n+1} - \tilde{\mathsf{J}}_n\right)\,, \tag{8}$$

where the angular momentum $\tilde{\mathsf{J}}^{(i)}_n$ is defined as

$$\tilde{\mathsf{J}}^{(i)}_n := \int_{\Omega_0} \boldsymbol{\varphi}^{(i)}_n \times \rho_0\mathbf{v}^{(i)}_n\,\mathrm{d}\Omega_0\,. \tag{9}$$

This produces the conservation statement

$$\boxed{\boldsymbol{\xi} \bullet \left(\tilde{\mathsf{J}}^{(i+1)}_{n+1} - \tilde{\mathsf{J}}_n\right) \;+\; \hat{\boldsymbol{\xi}}\Delta\mathrm{t} \bullet \int_{\Omega_0} \mathbf{F}^{(i)}_{n+1/2}\mathbf{S}^{(i)}_{n+1/2}\mathbf{F}^{(i+1)T}_{n+1/2}\,\mathrm{d}\Omega_0 \;=\; 0\,.} \tag{10}$$

However, note that

$$\underbrace{\hat{\boldsymbol{\xi}}}_{\text{skew-symmetric}} \bullet \underbrace{\mathbf{F}^{(i)}_{n+1/2}\mathbf{S}^{(i)}_{n+1/2}\mathbf{F}^{(i+1)T}_{n+1/2}}_{\text{generally unsymmetric}} \neq 0 \,, \tag{11}$$

because of the mismatching iteration indices (i) and $(i+1)$. Thus

$$\boldsymbol{\xi} \bullet \left(\tilde{\mathsf{J}}^{(i+1)}_{n+1} - \tilde{\mathsf{J}}_n\right) \neq 0 \,. \tag{12}$$

Remarks 2.3.

1. The measure of angular momentum $\tilde{\mathsf{J}}^{(i)}_n$ as defined in equation (9) is not an exactly conserved quantity.
2. If the fixed-point iteration is driven to a converged state, so that $(i) \to \infty$ and $\|\boldsymbol{\varphi}^{(i+1)}_{n+1} - \boldsymbol{\varphi}^{(i)}_{n+1}\| \to 0$, then $\tilde{\mathsf{J}}^{(\infty)}_{n+1} = \tilde{\mathsf{J}}_n$, and angular momentum (9) is conserved.
3. In general, and assuming the fixed-point iteration converges at the rate outlined in Remark 4.5 for the non-linear case, one would expect that
$$\left\|\tilde{\mathsf{J}}^{(m)}_{n+1} - \tilde{\mathsf{J}}^{(\infty)}_{n+1}\right\| \leqslant \mathcal{O}\left(\Delta \mathrm{t}^{2m}\right) \,, \tag{13}$$
where $1 \leqslant (m) < \infty$ is the iteration count.

3 Incremental Objectivity

Consider again the momentum equation

$$\int_{\Omega_0} \delta\boldsymbol{\varphi} \bullet \rho_0(\mathbf{v}^{(i+1)}_{n+1} - \mathbf{v}_n)\,\mathrm{d}\Omega_0 \;+\; \Delta\mathrm{t}\int_{\Omega_0} \mathrm{GRAD}[\delta\boldsymbol{\varphi}] \bullet \mathbf{F}^{(i)}_{n+1/2}\mathbf{S}^{(i)}_{n+1/2}\,\mathrm{d}\Omega_0 \;=\; 0 \,. \tag{14}$$

An admissible choice for $\delta\boldsymbol{\varphi}$ is $\delta\boldsymbol{\varphi} = \frac{1}{2}\left(\mathbf{v}^{(i+1)}_{n+1} + \mathbf{v}_n\right)$. This yields

$$\frac{1}{2}\int_{\Omega_0} (\mathbf{v}^{(i+1)}_{n+1} + \mathbf{v}_n) \bullet \rho_0(\mathbf{v}^{(i+1)}_{n+1} - \mathbf{v}_n)\,\mathrm{d}\Omega_0 \;+\; \frac{1}{2}\Delta\mathrm{t}\int_{\Omega_0} \mathrm{GRAD}[\mathbf{v}^{(i+1)}_{n+1} + \mathbf{v}_n] \bullet \mathbf{F}^{(i)}_{n+1/2}\mathbf{S}^{(i)}_{n+1/2}\,\mathrm{d}\Omega_0 \;=\; 0 \,. \tag{15}$$

This simplifies to

$$\left[\mathsf{T}^{(i+1)}_{n+1} - \mathsf{T}_n\right] + \frac{1}{2}\Delta\mathrm{t}\int_{\Omega_0} \mathrm{GRAD}[\mathbf{v}^{(i+1)}_{n+1} + \mathbf{v}_n] \bullet \mathbf{F}^{(i)}_{n+1/2}\mathbf{S}^{(i)}_{n+1/2}\,\mathrm{d}\Omega_0 \;=\; 0 \,, \tag{16}$$

where the total kinetic energy is defined as

$$\mathsf{T}^{(i)}_n := \frac{1}{2}\int_{\Omega_0} \rho_0 \|\mathbf{v}^{(i)}_n\|^2\,\mathrm{d}\Omega_0 \,. \tag{17}$$

Next, recall that

$$\boldsymbol{\varphi}^{(i+1)}_{n+1} - \boldsymbol{\varphi}_n = \Delta\mathrm{t}\cdot\mathbf{v}^{(i+1)}_{n+1/2} = \frac{1}{2}\Delta\mathrm{t}\cdot(\mathbf{v}^{(i+1)}_{n+1} + \mathbf{v}_n) \,. \tag{18}$$

This can be substituted into equation (16) producing

$$\left[\mathsf{T}^{(i+1)}_{n+1} - \mathsf{T}_n\right] \;+\; \int_{\Omega_0} (\mathbf{F}^{(i+1)}_{n+1} - \mathbf{F}_n) \bullet \mathbf{F}^{(i)}_{n+1/2}\mathbf{S}^{(i)}_{n+1/2}\,\mathrm{d}\Omega_0 \;=\; 0 \,. \tag{19}$$

This equation represents the change in kinetic energy from the previous time step to the current iteration of the current time step. Consistent with this, and to ensure conservation of total energy during the iterative process, the specific internal energy per unit mass $\varepsilon > 0$ is updated as

$$\left.\begin{aligned} \rho_0(\varepsilon^{(i+1)}_{n+1} - \varepsilon_n) \;&=\; (\mathbf{F}^{(i+1)}_{n+1} - \mathbf{F}_n) \bullet \mathbf{F}^{(i)}_{n+1/2}\mathbf{S}^{(i)}_{n+1/2} \\ &=\; \mathbf{F}^{(i)^T}_{n+1/2}(\mathbf{F}^{(i+1)}_{n+1} - \mathbf{F}_n) \bullet \mathbf{S}^{(i)}_{n+1/2} \end{aligned}\right\} \,. \tag{20}$$

Noting that

$$\mathbf{F}_{n+1/2}^{(i)} = \frac{1}{2}\left(\mathbf{F}_{n+1}^{(i)} + \mathbf{F}_n\right) , \tag{21}$$

this can be algebraically expanded to yield

$$\rho_0(\varepsilon_{n+1}^{(i+1)} - \varepsilon_n) \;=\; \frac{1}{2}\left(\mathbf{F}_{n+1}^{(i)^T}\mathbf{F}_{n+1}^{(i+1)} - \mathbf{F}_{n+1}^{(i)^T}\mathbf{F}_n + \mathbf{F}_n^T\mathbf{F}_{n+1}^{(i+1)} - \mathbf{F}_n^T\mathbf{F}_n\right) \bullet \mathbf{S}_{n+1/2}^{(i)} . \tag{22}$$

Consider initially the limit case as $(i) \to \infty$ and the fixed-point iteration converges. Then,

$$\rho_0(\varepsilon_{n+1} - \varepsilon_n) \;=\; \frac{1}{2}\left(\mathbf{F}_{n+1}^T\mathbf{F}_{n+1} \underbrace{-\mathbf{F}_{n+1}^T\mathbf{F}_n + \mathbf{F}_n^T\mathbf{F}_{n+1}}_{\text{skew}} - \mathbf{F}_n^T\mathbf{F}_n\right) \bullet \mathbf{S}_{n+1/2} . \tag{23}$$

Recalling that $\mathbf{S}$ is symmetric and the symmetric right Cauchy-Green strain is defined as $\mathbf{C} := \mathbf{F}^T\mathbf{F}$, this simplifies to

$$\rho_0(\varepsilon_{n+1} - \varepsilon_n) \;=\; \frac{1}{2}\left(\mathbf{C}_{n+1} - \mathbf{C}_n\right) \bullet \mathbf{S}_{n+1/2} . \tag{24}$$

Assume that the incremental motion over the time step $\Delta\mathrm{t}$ is a rigid rotation. Then $\mathbf{F}_{n+1} = \mathbf{Q}\mathbf{F}_n$ for some $\mathbf{Q} \in SO(3)$. This implies that $\mathbf{C}_{n+1} = \mathbf{C}_n$ and thus $\varepsilon_{n+1} = \varepsilon_n$.

Now consider the non-limit case where $(i) < \infty$ and the fixed-point iteration is not converged. Then

$$\rho_0(\varepsilon_{n+1}^{(i+1)} - \varepsilon_n) \;=\; \frac{1}{2}\left(\underbrace{\mathbf{F}_{n+1}^{(i)^T}\mathbf{F}_{n+1}^{(i+1)}}_{\neq \mathbf{C}_{n+1}^{(i+1)}} - \mathbf{C}_n - \underbrace{\mathbf{F}_{n+1}^{(i)^T}\mathbf{F}_n + \mathbf{F}_n^T\mathbf{F}_{n+1}^{(i+1)}}_{\text{not skew}}\right) \bullet \mathbf{S}_{n+1/2}^{(i)} . \tag{25}$$

This equation cannot easily be simplified any further due to the "mismatching" terms involving (i) and $(i+1)$.

Remarks 3.1.

1. The predictor-corrector algorithm is incrementally objective if the fixed-point iteration is driven to convergence.
2. In the case of a non-converged iterative process, the algorithm is not exactly incrementally objective. However, assuming the fixed-point iteration converges at the rate outlined in Remark 4.5 for the non-linear case, the internal energy evolves subject to the bound

$$\int_{\Omega_0} \rho_0 \|\varepsilon_{n+1}^{(m)} - \varepsilon_{n+1}^{(\infty)}\| \, \mathrm{d}\Omega_0 \;\leqslant\; \mathcal{O}\left(\Delta\mathrm{t}^{2m}\right) , \tag{26}$$

   where $1 \leqslant (m) < \infty$ is the iteration count.

4 Linearized (ODE) Algorithm

4.1 Stability

Consider a one-dimensional damped harmonic oscillator. The equation(s) of motion for this system can be written in first order form as

$$\frac{\mathrm{d}}{\mathrm{dt}}\begin{bmatrix} u \\ v \end{bmatrix} = \begin{bmatrix} 0 & 1 \\ -\omega^2 & -2\xi\omega \end{bmatrix}\begin{bmatrix} u \\ v \end{bmatrix} . \tag{27}$$

In the above equation, u is position, v is velocity, $w > 0$ is the undamped angular frequency and $\xi \geqslant 0$ is the (physical) damping ratio. For notational convenience, denote $\mathbf{z} = [u, v]^T$.

The midpoint predictor-corrector time integrator can be derived for this simple system from an operator splitting approach. First, the velocity is updated as

$$\left.\begin{aligned} v_{n+1}^{(i+1)} &= v_n - 2\xi\omega\Delta\mathrm{t}\, v_{n+1/2}^{(i)} - \omega^2\Delta\mathrm{t}\, u_{n+1/2}^{(i)} \\ &= v_n - \xi\omega\Delta\mathrm{t}\left(v_n + v_{n+1}^{(i)}\right) - \frac{1}{2}\omega^2\Delta\mathrm{t}\left(u_n + u_{n+1}^{(i)}\right) \\ &= (1-\xi\omega\Delta\mathrm{t})v_n - \frac{1}{2}\omega^2\Delta\mathrm{t}\, u_n - \xi\omega\Delta\mathrm{t}\, v_{n+1}^{(i)} - \frac{1}{2}\omega^2\Delta\mathrm{t}\, u_{n+1}^{(i)} \\ &= \mathbf{a}_0^T\mathbf{z}_n + \mathbf{a}_1^T\mathbf{z}_{n+1}^{(i)} \end{aligned}\right\}, \tag{28}$$

where

$$\mathbf{a}_0 := \left[-\frac{1}{2}\omega^2\Delta\mathrm{t}, 1-\xi\omega\Delta\mathrm{t}\right], \tag{29}$$

and

$$\mathbf{a}_1 := \left[-\frac{1}{2}\omega^2\Delta\mathrm{t}, -\xi\omega\Delta\mathrm{t}\right]. \tag{30}$$

The next step updates the position as

$$\left.\begin{aligned} u_{n+1}^{(i+1)} &= u_n + \Delta\mathrm{t}\, v_{n+1/2}^{(i+1)} \\ &= u_n + \frac{1}{2}\Delta\mathrm{t}\,\left(v_n + v_{n+1}^{(i+1)}\right) \\ &= u_n + \frac{1}{2}\Delta\mathrm{t}\, v_n + \frac{1}{2}\Delta v_{n+1}^{(i+1)} \\ &= \mathbf{b}_0^T\mathbf{z}_n + \frac{1}{2}\Delta\mathrm{t}\left(\mathbf{a}_0^T\mathbf{z}_n + \mathbf{a}_1^T\mathbf{z}_{n+1}^{(i)}\right) \\ &= \left(\mathbf{b}_0 + \frac{1}{2}\Delta\mathrm{t}\,\mathbf{a}_0\right)^T\mathbf{z}_n + \frac{1}{2}\Delta\mathrm{t}\,\mathbf{a}_1^T\mathbf{z}_{n+1}^{(i)} \end{aligned}\right\}, \tag{31}$$

where

$$\mathbf{b}_0 := \left[1, \frac{1}{2}\Delta\mathrm{t}\right]. \tag{32}$$

This leads to the system of equations

$$\mathbf{z}_{n+1}^{(i+1)} = \mathbf{A}_0\mathbf{z}_n + \mathbf{A}_1\mathbf{z}_{n+1}^{(i)}, \tag{33}$$

where

$$\mathbf{A}_0 := \begin{bmatrix} \mathbf{b}_0 + \frac{1}{2}\Delta\mathrm{t}\,\mathbf{a}_0 \\ \\ \mathbf{a}_0 \end{bmatrix}, \tag{34}$$

and

$$\mathbf{A}_1 := \begin{bmatrix} \frac{1}{2}\Delta\mathrm{t}\,\mathbf{a}_1 \\ \\ \mathbf{a}_1 \end{bmatrix}. \tag{35}$$

Two fixed point iterations are applied to produce

$$\left.\begin{aligned} \mathbf{z}_{n+1}^{(1)} &= \mathbf{A}_0\mathbf{z}_n + \mathbf{A}_1\mathbf{z}_n \\ &= (\mathbf{A}_0 + \mathbf{A}_1)\,\mathbf{z}_n \end{aligned}\right\}, \tag{36}$$

$$\left.\begin{aligned} \mathbf{z}_{n+1}^{(2)} &= \mathbf{A}_0\mathbf{z}_n + \mathbf{A}_1\mathbf{z}_{n+1}^{(1)} \\ &= \mathbf{A}_0\mathbf{z}_n + \mathbf{A}_1\,(\mathbf{A}_0 + \mathbf{A}_1)\,\mathbf{z}_n \\ &= \left[\mathbf{A}_0 + \mathbf{A}_1\,(\mathbf{A}_0 + \mathbf{A}_1)\right]\mathbf{z}_n \\ &=: \mathbf{A}\mathbf{z}_n \end{aligned}\right\}. \tag{37}$$

In the above, the 2×2 matrix $\mathbf{A}$ is the *amplification* matrix.

Remarks 4.1. One can show analytically, and verify numerically, that the eigenvalues of $\mathbf{A}$ depend only upon the dimensionless quantities

$$\Omega := \omega \Delta \mathrm{t}$$

and ξ [17, 18]. The algebraic details, being somewhat tedious, are omitted.

The properties of the amplification matrix fully determine the stability properties of the algorithm. Stability requires that $\|\mathbf{A}\| \leqslant 1$, where

$$\|\mathbf{A}\| := \max_{\mathbf{z} \in \mathbb{R}^2} \frac{\|\mathbf{A}\mathbf{z}\|}{\|\mathbf{z}\|} \ . \tag{38}$$

The spectral radius of $\mathbf{A}$ is defined as

$$\rho(\mathbf{A}) := \max\left\{|\lambda_1|, |\lambda_2|\right\} \ , \tag{39}$$

where $\lambda_1, \lambda_2 \in \mathbb{C}$ are the (complex) eigenvalues of $\mathbf{A}$. In general $\rho(\mathbf{A}) \leqslant \|\mathbf{A}\|$. However [10, section 4.9.2],

$$\left.\begin{array}{lll} \rho(\mathbf{A}) > 1 & \Longleftrightarrow & \lim\limits_{n\to\infty} \|\mathbf{A}^n\| = \infty \qquad \text{(instability)} \\ \rho(\mathbf{A}) < 1 & \Longleftrightarrow & \lim\limits_{n\to\infty} \|\mathbf{A}^n\| = 0 \qquad \text{(stability)} \end{array}\right\} \ . \tag{40}$$

The case when $\rho(\mathbf{A}) = 1$ is more complicated. The spectral radius has the property [34, section 4.4]

$$\rho(\mathbf{A}) = \lim_{n\to\infty} \|\mathbf{A}^n\|^{1/n} \ . \tag{41}$$

When $\rho(\mathbf{A}) = 1$ this implies that $\lim_{n\to\infty} \|\mathbf{A}^n\|^{1/n} = 1$. This allows for linear growth, i.e., $\|\mathbf{A}^n\| \propto n$. Nevertheless, the (weaker) stability condition adopted in this work is $\rho(\mathbf{A}) \leqslant 1$.

There are two values of Ω which are of interest:

- Denote by Ω_{crit} the smallest value of Ω for which at least one of the eigenvalues of $\mathbf{A}$ has modulus greater than 1. This is the absolute stability limit.
- The eigenvalues of $\mathbf{A}$ are either complex conjugates or real. Denote by Ω_{bif} the smallest value of Ω for which the eigenvalues are real. In other words, with increasing Ω from zero, the eigenvalues bifurcate from complex conjugates to real when $\Omega = \Omega_{\text{bif}}$. When $\Omega < \Omega_{\text{bif}}$, the eigenvalues are complex conjugates; when $\Omega > \Omega_{\text{bif}}$ the eigenvalues are real. In general $\Omega_{\text{bif}} \leqslant \Omega_{\text{crit}}$, which is typical for explicit predictor-corrector algorithms [19].

MATLAB® ™ [14, 15] is used to numerically calculate the amplification matrix $\mathbf{A}$ and extract the eigenvalues. The plots in this section are generated with that software package. Figure 1 is a plot of the eigenvalues of $\mathbf{A}$ versus Ω. Table 4.1 is a table of approximate values of Ω_{bif} and Ω_{crit} for chosen discrete values of the damping ratio ξ. Table 4.1 is a table of approximate values of Ω_{bif} and Ω_{crit} for large values of the damping ratio ξ. The values of $(1/\xi)$ are also included in the table. Clearly,

$$\boxed{\xi \nearrow \infty \quad \Longrightarrow \quad \Omega_{\text{crit}} \searrow \frac{1}{\xi} \ .} \tag{42}$$

Remarks 4.2. The following are consistent with remarks made in [17, 18] and can be inferred from the data presented here:

1. Increasing the damping factor ξ decreases both the critical and bifurcation time steps.
2. Choosing $\Omega = \Omega_{\text{bif}}$ maximizes the algorithmic (high frequency) numerical dissipation. Generally speaking, numerical results are more satisfactory when $\Omega \leqslant \Omega_{\text{bif}}$. This is a tighter time-step restriction than stability, which only requires that $\Omega \leqslant \Omega_{\text{crit}}$.

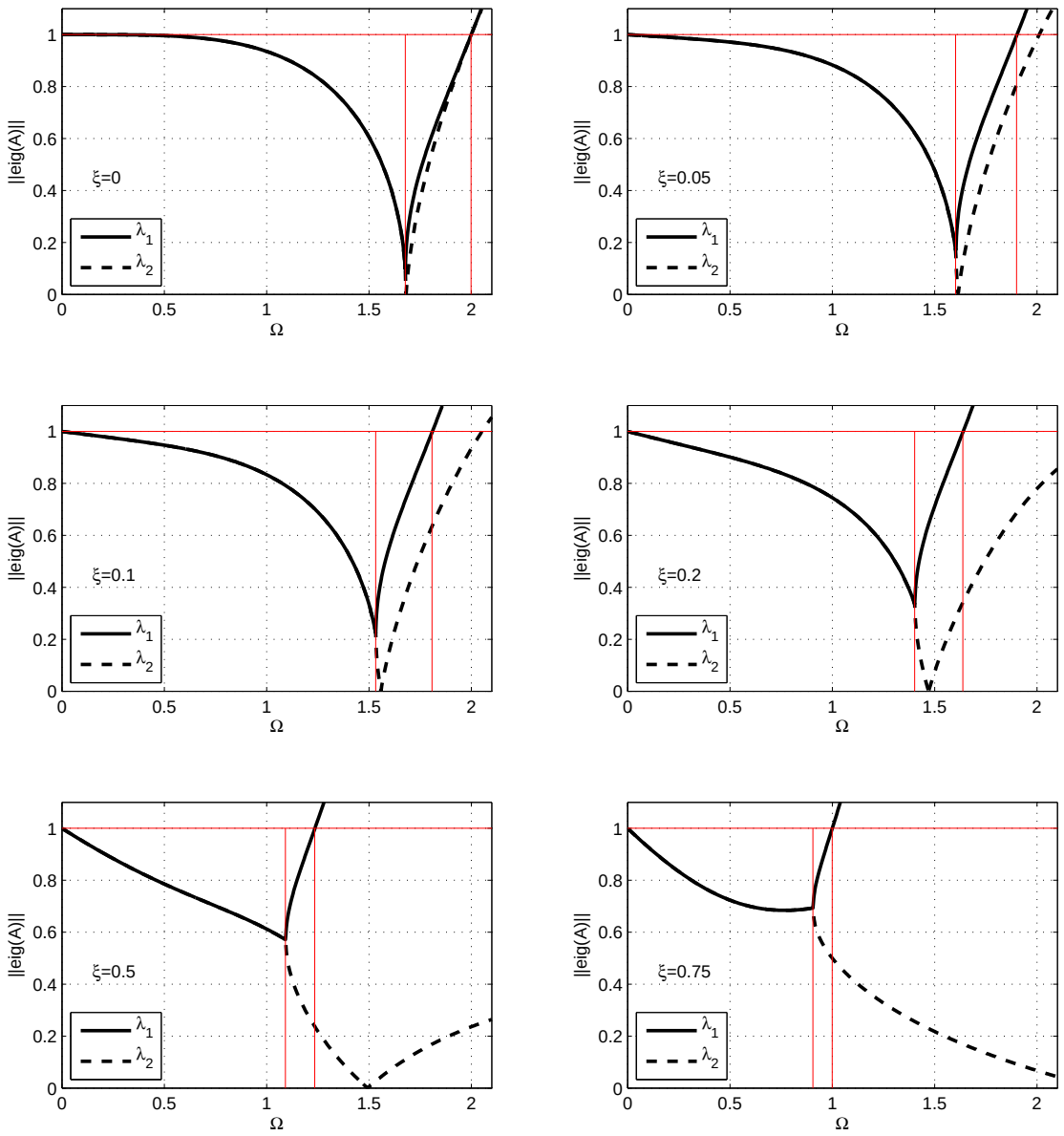

Figure 1. Modulus of the eigenvalues of $\mathbf{A}$ versus Ω for increasing values of the damping ratio ξ. The (red) vertical lines denote Ω_{bif} and Ω_{crit}, respectively. The (red) horizontal line at 1 represents the stability limit.

ξ	$\Omega_{\rm crit}$	$\Omega_{\rm bif}$
0.0	2.00	1.67
0.05	1.90	1.60
0.10	1.80	1.53
0.20	1.63	1.40
0.50	1.23	1.09
0.75	0.99	0.90
1.0	0.83	0.76
2.0	0.47	0.45

Table 1. Approximate values of $\Omega_{\rm crit}$ and $\Omega_{\rm bif}$ for increasing values of ξ.

3. For the *central-difference method* as described in [18], $\Omega_{\rm crit} = 2\ \forall \xi \geqslant 0$. However, there is an alternative central-difference method, described in [3, 9, 16, 38], in which the damping term $(2\xi\omega v)$ is lagged by a half time-step with respect to the other terms. That is also the algorithm used in ALEGRA [25]. For that version of the method,
$$\Omega_{\rm crit} = 2\left(\sqrt{1+\xi^2} - \xi\right) \leqslant 2\ .$$
There are multiple ways of lagging in time the damping term, all of which reduce the numerical stability limit [28]. In any case, when $\xi = 0$, $\Omega_{\rm bif} = 2$.

4. For the midpoint predictor-corrector algorithm, when $\xi = 0$, $\Omega_{\rm crit} = 2$, the same as for the central-difference method. However, $\Omega_{\rm bif} \approx 1.67 < 2$.

5. For a two-node one-dimensional lumped mass finite element, the maximum frequency is $\omega_{\max} = 2c/h$, where $c > 0$ is the material sound speed and $h > 0$ is the element length [17, 18]. Thus for stability,
$$\frac{2c}{h}\Delta{\rm t} \leqslant \Omega_{\rm crit} \quad \Longleftrightarrow \quad \Delta{\rm t} \leqslant \frac{\Omega_{\rm crit}}{2}\cdot\frac{h}{c}\ ,$$
and for high frequency dissipation
$$\frac{2c}{h}\Delta{\rm t} \leqslant \Omega_{\rm bif} \quad \Longleftrightarrow \quad \Delta{\rm t} \leqslant \frac{\Omega_{\rm bif}}{2}\cdot\frac{h}{c}\ .$$

Using the symbolic manipulation software package MATHEMATICA® ™ [1, 39] a closed form expression for $\mathbf{A}$ can be developed. The result is

$$\mathbf{A} = \begin{bmatrix} 1 - \frac{1}{2}\omega^2\Delta{\rm t}^2 + \frac{1}{2}\xi\omega^3\Delta{\rm t}^3 + \frac{1}{8}\omega^4\Delta{\rm t}^4 & \Delta{\rm t} - \xi\omega\Delta{\rm t}^2 - \frac{1}{4}\omega^2\Delta{\rm t}^3 + \xi^2\omega^2\Delta{\rm t}^3 + \frac{1}{4}\xi\omega^3\Delta{\rm t}^4 \\ -\omega^2\Delta{\rm t} + \xi\omega^3\Delta{\rm t}^2 + \frac{1}{4}\omega^4\Delta{\rm t}^3 & 1 - 2\omega\xi\Delta{\rm t} - \frac{1}{2}\omega^2\Delta{\rm t}^2 + 2\xi^2\omega^2\Delta{\rm t}^2 + \frac{1}{2}\xi\omega^3\Delta{\rm t}^3 \end{bmatrix}\ . \tag{43}$$

The eigenvalues of $\mathbf{A}$ are
$$\lambda_{1,2} = \frac{1}{16}\left(\lambda_r \pm \sqrt{\lambda_i}\right)\ , \tag{44}$$
where
$$\lambda_r = 16 - 16\xi\Omega - 8\Omega^2 + 16\xi^2\Omega^2 + 8\xi\Omega^3 + \Omega^4\ , \tag{45}$$
and
$$\lambda_i = -32(8 - 16\xi\Omega + 16\xi^2\Omega^2 - \Omega^4)\ +\ \lambda_r^2\ . \tag{46}$$

ξ	$\Omega_{\rm crit}$	$\Omega_{\rm bif}$	$1/\xi$
2	4.721×10^{-1}	4.557×10^{-1}	5.000×10^{-1}
4	2.462×10^{-1}	2.432×10^{-1}	2.500×10^{-1}
8	1.245×10^{-1}	1.240×10^{-1}	1.250×10^{-1}
16	6.240×10^{-2}	0	6.250×10^{-2}
32	3.120×10^{-2}	0	3.125×10^{-2}
64	1.560×10^{-2}	0	1.5625×10^{-2}
128	7.800×10^{-3}	0	7.8125×10^{-3}
256	3.900×10^{-3}	0	3.9063×10^{-3}

Table 2. Approximate values of $\Omega_{\rm crit}$ and $\Omega_{\rm bif}$ for large values of ξ. Included in this table are values of $1/\xi$.

The critical value $\Omega_{\rm crit}$ occurs when $\max(|\lambda_1|, |\lambda_2|) = 1$ and the bifurcation value $\Omega_{\rm bif}$ occurs when $\lambda_i = 0$. Using MATHEMATICA® ™, the equation

$$\frac{1}{16}\left(\lambda_r + \sqrt{\lambda_i}\right) = +1\,, \tag{47}$$

can be solved for Ω, yielding three roots

$$\Omega = \left\{0,\ 2\left(-\sqrt{1+\xi^2} - \xi\right),\ 2\left(\sqrt{1+\xi^2} - \xi\right)\right\}\ . \tag{48}$$

Clearly only the third root is physically significant, and thus

$$\boxed{\Omega_{\rm crit} = 2\left(\sqrt{1+\xi^2} - \xi\right)\ = \frac{2}{\sqrt{1+\xi^2}+\xi}\,,} \tag{49}$$

the same as for the central-difference method. For $\xi \gg 1$, an asymptotic expansion yields

$$\Omega_{\rm crit} \quad \approx \quad \frac{1}{\xi} \ - \ \frac{1}{4}\left(\frac{1}{\xi}\right)^3 \ + \ \frac{1}{8}\left(\frac{1}{\xi}\right)^5 \ + \ \mathcal{O}\left(\frac{1}{\xi}\right)^6\ . \tag{50}$$

The solution to $\lambda_i = 0$ yields the bifurcation point

$$\left.\begin{aligned} \Omega_{\rm bif} = -\frac{4}{3}(1+2\xi) \ + \ \frac{1}{6}(16+16\xi+16\xi^2)A^{-1} \ + \ \frac{2}{3}A \\ \text{with} \quad A = \left(19+15\xi+12\xi^2+8\xi^3+3\sqrt{3}\sqrt{11+14\xi+11\xi^2+8\xi^3}\ \right)^{1/3} \end{aligned}\right\}\ . \tag{51}$$

For large $\xi \gg 1$, the asymptotic expansion is

$$\Omega_{\rm bif} \quad \approx \quad \frac{1}{\xi} \ - \ \frac{1}{2}\left(\frac{1}{\xi}\right)^3 \ + \ \frac{1}{4}\left(\frac{1}{\xi}\right)^4 \ + \ \frac{3}{16}\left(\frac{1}{\xi}\right)^5 \ + \ \mathcal{O}\left(\frac{1}{\xi}\right)^{11/2}\ . \tag{52}$$

4.2 Dissipation and Dispersion

Following the developments in [11] let $\lambda \in \mathbb{C}$ be a eigenvalue of the amplification matrix $\mathbf{A}$. Since λ is complex, it can be written in the form

$$\lambda = \exp(\alpha \Delta \mathrm{t}) \quad \text{with} \quad \alpha = -\bar{\xi} + \mathrm{i}\,\bar{\omega}\,. \tag{53}$$

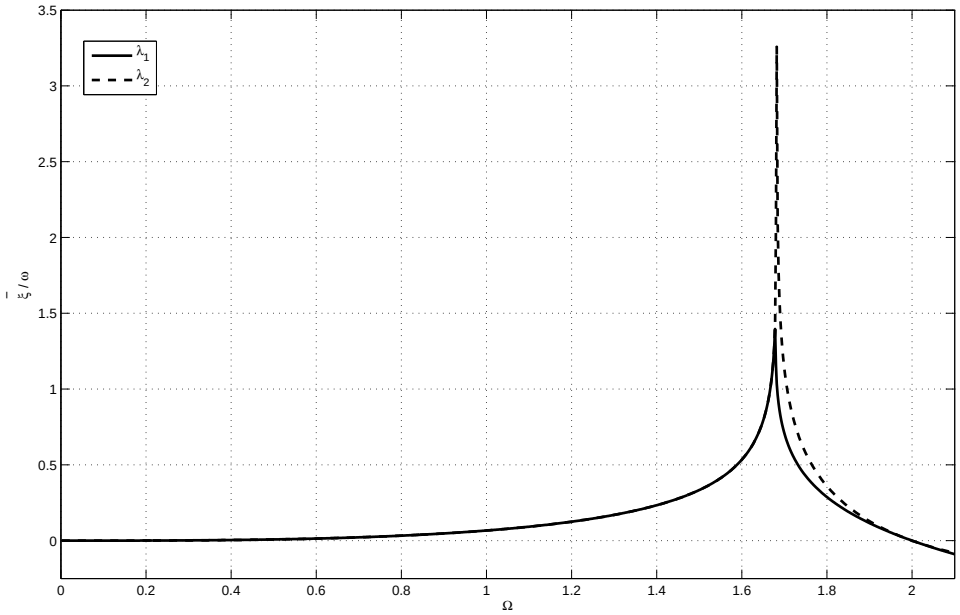

Figure 2. Relative dissipation $\left(\bar{\xi}/\omega\right)$ versus Ω for the undamped case.

The goal is to compute $\bar{\xi}$ and $\bar{\omega}$, the algorithmic dissipation and algorithmic frequency, respectively. First note that

$$\left.\begin{aligned} |\lambda| &= |\exp(\alpha\Delta \mathrm{t})| \\ &= |\exp(-\bar{\xi}\Delta \mathrm{t}) \cdot \exp(\mathrm{i}\bar{\omega}\Delta \mathrm{t})| \\ &= |\exp(-\bar{\xi}\Delta \mathrm{t})| \cdot |\exp(\mathrm{i}\bar{\omega}\Delta \mathrm{t})| \\ &= \exp(-\bar{\xi}\Delta \mathrm{t}) \end{aligned}\right\} , \tag{54}$$

and thus

$$\bar{\xi} = -\frac{1}{\Delta \mathrm{t}} \log |\lambda| \, . \tag{55}$$

Next,

$$\left.\begin{aligned} \arg(\lambda) &= \arg\left[\exp(\alpha\Delta \mathrm{t})\right] \\ &= \arg\left[\exp(-\bar{\xi}\Delta \mathrm{t}) \cdot \exp(\mathrm{i}\bar{\omega}\Delta \mathrm{t})\right] \\ &= \arg\left[\exp(\mathrm{i}\bar{\omega}\Delta \mathrm{t})\right] \\ &= \bar{\omega}\Delta \mathrm{t} \end{aligned}\right\} , \tag{56}$$

so that

$$\bar{\omega} = \frac{1}{\Delta \mathrm{t}} \arg(\lambda) \, . \tag{57}$$

Note that $\bar{\xi}$ and $\bar{\omega}$ have units of $(\text{time})^{-1}$. They can be non-dimensionalized by ω; the ratios $\left(\bar{\xi}/\omega\right)$ and $(\bar{\omega}/\omega)$ are dimensionless. In particular, the ratio $(\bar{\omega}/\omega)$ is the *relative phase error* of the time integration algorithm. Figure 2 is a plot of the relative dissipation of the midpoint algorithm, and figure 3 is a plot of the relative phase error. The phase error plot is only shown for $\Omega < \Omega_{\text{bif}}$.

Remarks 4.3.

1. Note that the relative phase error $(\bar{\omega}/\omega) \leqslant 1$. This is in contrast with the central-difference method, for which $(\bar{\omega}/\omega) \geqslant 1$ [31, Figure 2a].

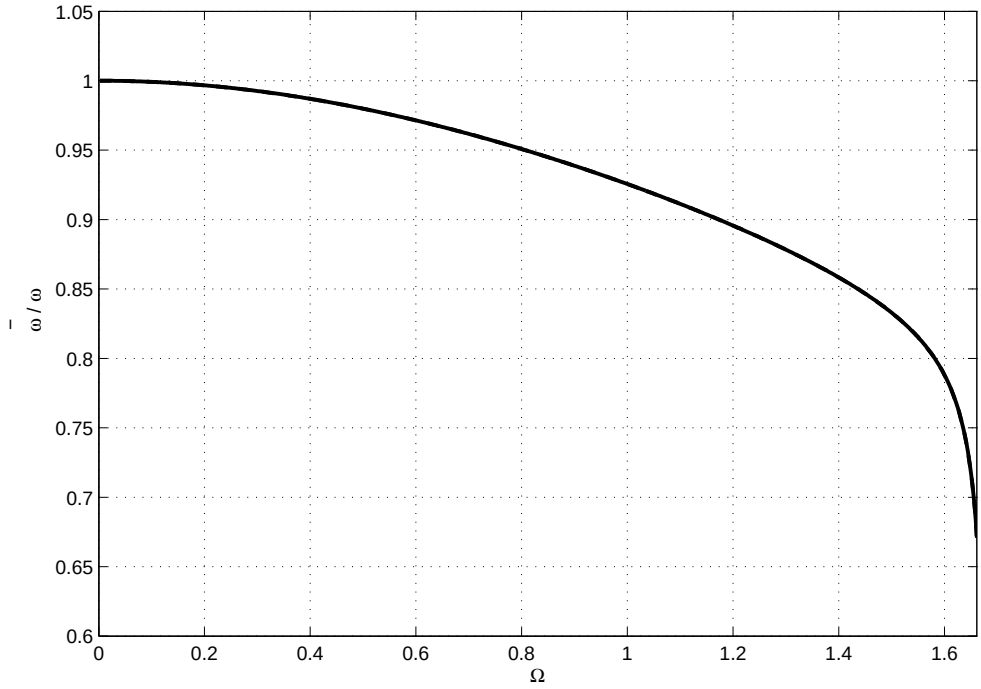

Figure 3. Relative phase error $(\bar{\omega}/\omega)$ versus Ω for the undamped case.

2. The phase error plot again motivates choosing $\Omega \leqslant \Omega_{\text{bif}}$. As $\Omega \to \Omega_{\text{bif}}$, the phase error $(\bar{\omega}/\omega) \to 0$, and the numerical accuracy severely deteriorates.

3. Again consider two-node one-dimensional lumped mass finite elements. Let ω^h be the time-continuous, spatially discrete harmonic frequency of oscillation for wavenumber $k > 0$. The exact, time- and space- continuous harmonic frequency is of course $\omega = kc$. In this setting, $(\omega^h/\omega) \leq 1$ [18, Section 9.1.4]. For the central-difference method the spatial and temporal phase errors have the potential to cancel each other in the sense that

$$\underbrace{\left(\frac{\bar{\omega}^h}{\omega^h}\right)}_{\geqslant 1} \cdot \underbrace{\left(\frac{\omega^h}{\omega}\right)}_{\leqslant 1} = 1 \ ,$$

when $\Delta \mathrm{t} = h/c$ (the *CFL* stability limit) [18, 31]. Lumped mass finite elements and the central-difference method are matched [18, 23]. On the other hand, for the midpoint predictor-corrector approach

$$\underbrace{\left(\frac{\bar{\omega}^h}{\omega^h}\right)}_{\leqslant 1} \cdot \underbrace{\left(\frac{\omega^h}{\omega}\right)}_{\leqslant 1} \leqslant 1 \ .$$

The midpoint time integrator and lumped mass finite elements are not matched.

4.3 Three Iterations

The midpoint predictor-corrector algorithm can be run with three or more iterations. For the three iteration case, the amplification matrix $\mathbf{A}$ has the form

$$\mathbf{A} = \mathbf{A}_0 \ + \ \mathbf{A}_1 \left[\mathbf{A}_0 + \mathbf{A}_1 \left(\mathbf{A}_0 + \mathbf{A}_1\right)\right] \ . \tag{58}$$

ξ	Ω_{crit}
0.0	0
0.05	1.12
0.10	1.22
0.20	1.31
0.50	1.58
0.75	1.15
1.0	0.91
2.0	0.48
64	0.0156
256	0.0039

Table 3. Three iteration case: Approximate values of Ω_{crit} for increasing values of ξ.

Figure 4 is a plot of the eigenvalues of $\mathbf{A}$ versus Ω. Table 4.3 is a table of approximate values of Ω_{crit} for chosen discrete values of the damping ratio ξ. Figure 5 is a plot of the relative dissipation of the algorithm, and figure 6 is a plot of the relative phase error, both for the undamped case.

Using MATHEMATICA® ™, the eigenvalues of $\mathbf{A}$, when $\xi = 0$, have the closed form expression

$$\lambda_{1,2} = \frac{1}{64}\left(\lambda_r \pm \sqrt{\lambda_i}\right) , \tag{59}$$

where

$$\lambda_r = 64 - 32\Omega^2 + 8\Omega^4 - \Omega^6 , \tag{60}$$

and

$$\lambda_i = -128\left(32 + \Omega^6\right) + \left(-64 + 32\Omega^2 - 8\Omega^4 + \Omega^6\right)^2 . \tag{61}$$

Note that $\lambda_i \leqslant 0 \ \ \forall\, \Omega \leqslant 3$, which implies that the eigenvalues are complex conjugates and

$$|\lambda_{1,2}| = \frac{1}{64}\sqrt{\left(\lambda_r^2 - \lambda_i\right)} . \tag{62}$$

When $\Omega \ll 1$, $|\lambda_{1,2}|$ has the asymptotic expansion

$$|\lambda_{1,2}| \ \approx \ 1 \ + \ \frac{\Omega^6}{64} \ + \ \mathcal{O}(\Omega^{12}) \ \geqslant 1 . \tag{63}$$

Remarks 4.4. The following can be inferred from the data presented:

1. The algorithm run with three iterations is *unconditionally unstable* when $\xi = 0$. The instability has order $[1 + \mathcal{O}(\Delta t^6)]$.
2. The introduction of physical damping helps stabilize the algorithm. However, $\xi \nearrow \infty \implies \Omega_{\text{crit}} \searrow (1/\xi)$, which is to be expected.
3. Ironically, and despite the instability, the phase error is improved for large Ω with respect to the two-iteration case.

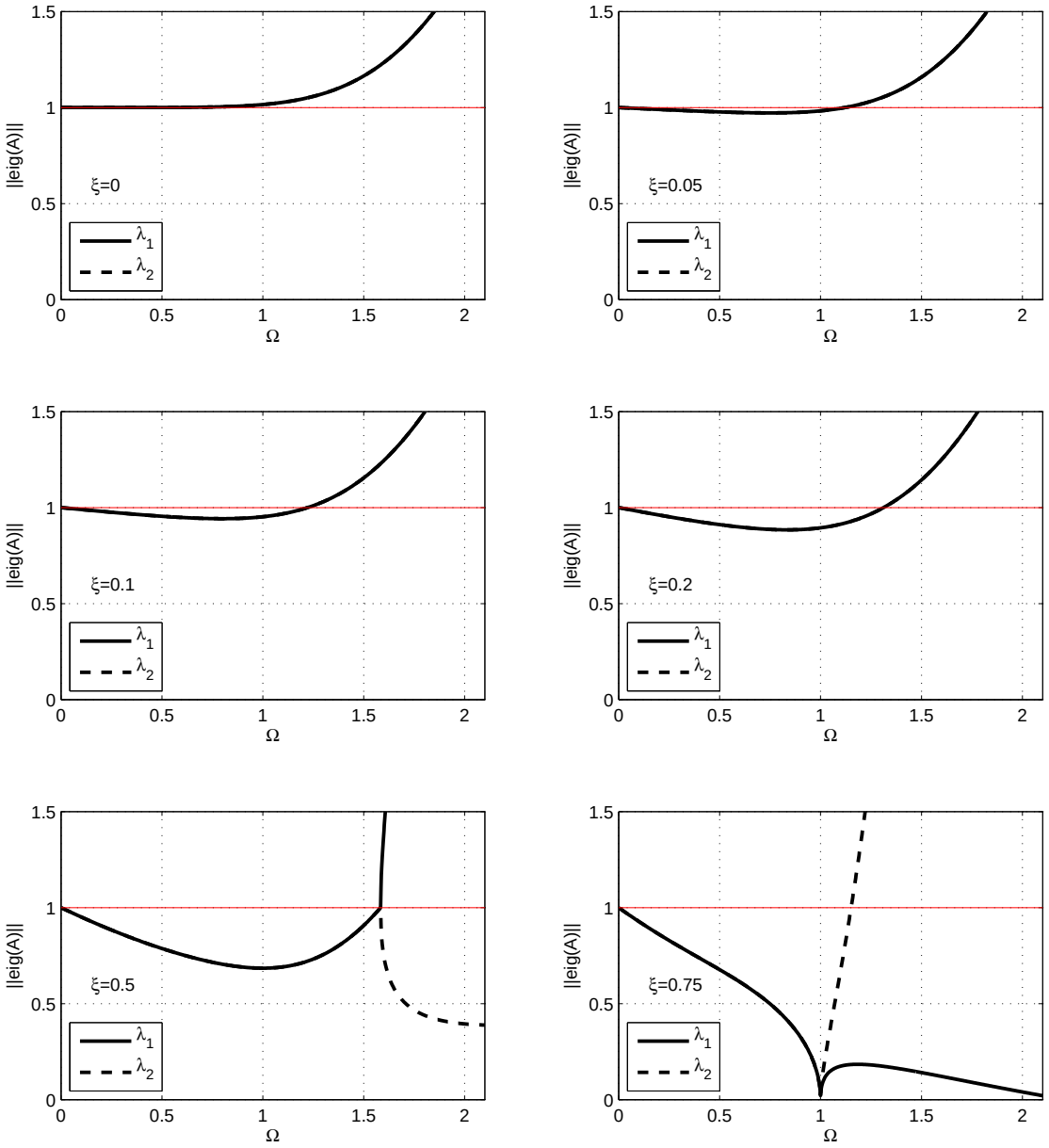

Figure 4. Three iteration case: Modulus of the eigenvalues of $\mathbf{A}$ versus Ω for increasing values of the damping ratio ξ. The (red) horizontal line at 1 represents the stability limit.

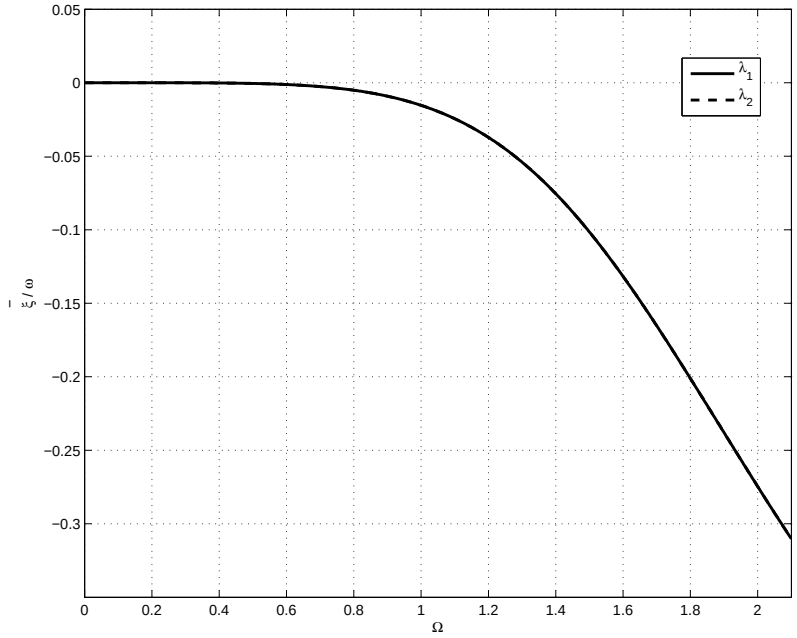

Figure 5. Three iteration case: Relative dissipation $\left(\bar{\xi}/\omega\right)$ versus Ω for the undamped case. The instability is clear since $\bar{\xi} \leqslant 0$.

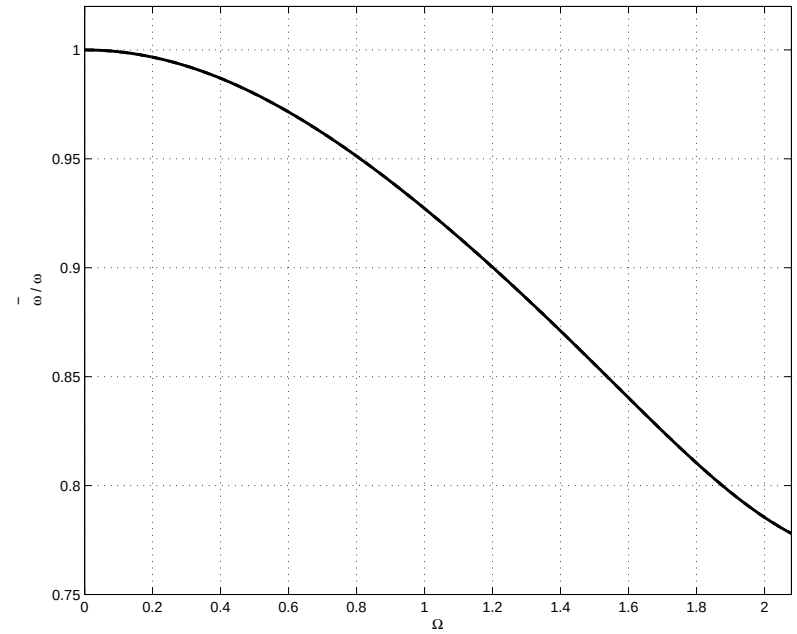

Figure 6. Three iteration case: Relative phase error $(\bar{\omega}/\omega)$ versus Ω for the undamped case.

Remarks 4.5. For the undamped case, and for an increasing number of iterations, the leading order terms in the Taylor series expansion of $|\lambda_{1,2}|$ have the form

$$|\lambda_{1,2}| \;\approx\; 1 \;+\; M(-1)^{(j-1)}\left(\frac{\Omega}{2}\right)^{2j} \;+\; \ldots \quad \text{(for some } 0 < M < \infty) \;, \tag{64}$$

where $(j) \geqslant 1$ is the iteration count. Thus when (j) is even the algorithm is (conditionally) stable; when (j) is odd the algorithm is unstable. Note that when $\Omega < 2$, $\lim_{j\to\infty} |\lambda_{1,2}| = 1$. See also section 4.4.

4.4 Convergence of the Fixed Point Iteration

. Consider the fixed point iteration

$$\mathbf{z}_{n+1}^{(i+1)} = \mathbf{A}_1 \mathbf{z}_{n+1}^{(i)} + \mathbf{A}_0 \mathbf{z}_n \;. \tag{65}$$

The goal of this sub-section is to examine the limiting situation where $i \nearrow \infty$. For notational convenience, denote $\mathbf{x}^{(i)} := \mathbf{z}_{n+1}^{(i)}$ and $\mathbf{b} := \mathbf{A}_0 \mathbf{z}_n$ so that the above fixed-point iteration can be written as

$$\mathbf{x}^{(i+1)} = \mathbf{A}_1 \mathbf{x}^{(i)} + \mathbf{b} \;. \tag{66}$$

For the midpoint predictor-corrector algorithm, the matrix $\mathbf{A}_1$ has the closed form expression

$$\mathbf{A}_1 = \begin{bmatrix} -\frac{1}{4}\omega^2 \Delta \mathrm{t}^2 & -\frac{1}{2}\xi\omega\Delta \mathrm{t}^2 \\ \\ -\frac{1}{2}\omega^2 \Delta \mathrm{t} & -\xi\omega\Delta \mathrm{t} \end{bmatrix} \;. \tag{67}$$

The eigenvalues of $\mathbf{A}_1$ are

$$\mathrm{eig}(\mathbf{A}_1) = \left\{ 0, -\frac{1}{4}(\Omega^2 + 4\xi\Omega) \right\} \;. \tag{68}$$

When $\Omega > 0$ the eigenvalues of $\mathbf{A}_1$ are real and distinct and thus $\mathbf{A}_1$ is (real) diagonalizable [13]. This also ensures that $\rho(\mathbf{A}_1) = \|\mathbf{A}_1\|$. A sufficient condition for the fixed-point iteration (66) to converge, and for $(\mathbf{I} - \mathbf{A}_1)$ to be non-singular, is that $\|\mathbf{A}_1\| < 1$ [20, 22]. The converged solution is $\mathbf{x}^* := (\mathbf{I} - \mathbf{A}_1)^{-1}\mathbf{b}$. Examining the condition that $\|\mathbf{A}_1\| < 1$ yields

$$\|\mathbf{A}_1\| < 1 \Longleftrightarrow \rho(\mathbf{A}_1) < 1 \Longleftrightarrow \frac{1}{4}(\Omega^2 + 4\xi\Omega) < 1 \Longleftrightarrow \Omega < 2\left(\sqrt{1+\xi^2} - \xi\right) \;, \tag{69}$$

almost the same as the stability criteria. Thus if this condition holds

$$\lim_{i\nearrow\infty} \|\mathbf{x}^{(i)} - \mathbf{x}^*\| = 0 \;, \tag{70}$$

and the convergence is *q-linear* [20], with q-factor $\|\mathbf{A}_1\| < 1$, in the sense that

$$\|\mathbf{x}^{(i+1)} - \mathbf{x}^*\| \leqslant \|\mathbf{A}_1\| \cdot \|\mathbf{x}^{(i)} - \mathbf{x}^*\| \;, \tag{71}$$

in the limit as $i \nearrow \infty$.

Remarks 4.6.

1. The condition $\Omega = 2\left(\sqrt{1+\xi^2} - \xi\right)$ is the absolute stability condition, but is not sufficient to ensure convergence of the fixed-point iteration.
2. Given that the convergence rate is linear, it may not be computationally tractable to drive the iterations to convergence.
3. Numerical experiments indicate than an *even number of iterations is conditionally stable* (when $\xi = 0$), with algorithmic properties similar to the two-iteration case. Analogously, numerical experiments demonstrate that an *odd number of iterations is (mildly) unstable* (when $\xi = 0$), with algorithmic properties similar to the three-iteration case.
4. If the fixed-point iteration is converged then stability is recovered. This may of course require many iterations, particularly when $\rho(\mathbf{A}_1) \approx 1$.

5 Linearized (PDE) Algorithm

5.1 Linearized Gas Dynamics

The equations of linearized Lagrangian gas dynamics can be written as

$$\frac{\mathrm{d}}{\mathrm{dt}} \begin{bmatrix} u \\ v \\ p \end{bmatrix} = \begin{bmatrix} v \\ -p_x + \nu v_{xx} \\ -c^2 v_x \end{bmatrix} , \tag{72}$$

where u is position, v is velocity, p is the kinematic pressure (physical pressure divided by density), $\nu \geqslant 0$ is the kinematic viscosity (physical viscosity divided by density) and $c > 0$ is the reference sound speed. These equations are hyperbolic and admit wave-type solutions.

Towards the goal of a Fourier stability analysis [30, 36] assume all fields have a harmonic spatial variation

$$\begin{bmatrix} u(x,\mathrm{t}) \\ v(x,\mathrm{t}) \\ p(x,\mathrm{t}) \end{bmatrix} = \begin{bmatrix} u(\mathrm{t}) \\ v(\mathrm{t}) \\ p(\mathrm{t}) \end{bmatrix} \cdot \exp(\mathrm{i}kx) , \tag{73}$$

for wavenumber $k > 0$. This reduces the system of equations to

$$\frac{\mathrm{d}}{\mathrm{dt}} \begin{bmatrix} u \\ v \\ p \end{bmatrix} = \begin{bmatrix} v \\ -\mathrm{i}kp - \nu k^2 v \\ -\mathrm{i}kc^2 v \end{bmatrix} . \tag{74}$$

For notational convenience, denote $\mathbf{z} := [u, v, p]^T$.

Remarks 5.1. When $\nu = 0$:

1. The system of equations (74) admits solutions of the form

$$\begin{bmatrix} u(\mathrm{t}) \\ v(\mathrm{t}) \\ p(\mathrm{t}) \end{bmatrix} = \begin{bmatrix} u_0 \\ v_0 \\ p_0 \end{bmatrix} \cdot \exp(\mathrm{i}\omega\mathrm{t}) ,$$

   where $\omega = ck$.

2. The finite element (or finite difference) spatial discretization of equations (74) also admits solutions with a harmonic time dependence $\exp[\mathrm{i}\omega^h \mathrm{t}]$. However, any spatial discretization introduces dispersive effects, so that in general $\omega^h \neq ck$ [21, 27, 31].

3. It is not necessary to let $k \to \infty$ for a finite dimensional finite element system. Let $\mathbf{M}$ be the "mass" matrix and $\mathbf{K}$ be the "stiffness" of the finite element system. Let $\omega^h_{\max} \geqslant 0$ be the largest real root of

$$\det\left[\mathbf{K} - (\omega^h)^2 \mathbf{M}\right] = 0 .$$

   Then one need only consider wavenumbers $k \leqslant (\omega^h_{\max}/c)$.

4. For the two-node lumped mass element, $\omega_{\max} = (2c/h)$ so that $k_{\max} = (2/h)$.

Remarks 5.2. When $\nu > 0$:

1. Relative to section 4, the algorithmic damping ratio ξ can be computed as

$$2\xi\omega = 2\xi ck = \nu k^2 \quad \Longleftrightarrow \quad \xi = \frac{\nu k}{2c} .$$

   Thus ξ scales linearly with ν and k, and inversely with c.

2. The maximum algorithmic damping ratio can be computed as

$$\xi_{\max} \;=\; \frac{\nu}{2c} k_{\max} \;=\; \frac{\nu}{2c} \cdot \frac{2}{h} \;=\; \frac{\nu}{ch} \,.$$

3. For the fully non-linear problem [25, 32, 33], the artificial viscosity has the form

$$q = \rho \cdot h \left(c_1 c + c_2 h |\nabla \cdot \mathbf{v}| \right) \cdot \min\left(0, \nabla \cdot \mathbf{v}\right) \;,$$

with dimensionless constants $c_1 \geqslant 0$ and $c_2 \geqslant 0$. In this case the kinematic viscosity is

$$\nu = h \left(c_1 c + c_2 h |\nabla \cdot \mathbf{v}| \right) \;,$$

and thus

$$\xi_{\max} \;=\; \frac{\nu}{ch} \;=\; \left[c_1 + c_2 \frac{h}{c} |\nabla \cdot \mathbf{v}| \right] \,.$$

This equation is also derived in reference [38].

4. Since the equations with damping ($\nu > 0 \Longleftrightarrow \xi > 0$) have been considered in section 4, from this point forward it is assumed that $\nu = 0$.

5.2 Central-Difference Method

The central-difference method [3, 4, 25, 28] with parameter $\beta \in [0, 1]$, can be written as

$$\left.\begin{aligned} u_{n+1} &= u_n + v_{n+1/2}\Delta\mathrm{t} \\ v_{n+1/2} &= v_{n-1/2} - \mathrm{i}k\Delta\mathrm{t} p_n \\ p_{n+1} &= p_n - \mathrm{i}kc^2\Delta\mathrm{t}[(1-\beta)v_{n-1/2} + \beta v_{n+1/2}] \end{aligned}\right\} \,. \tag{75}$$

Note that this is equivalent to

$$\left.\begin{aligned} u_{n+1} &= u_n + v_{n+1}\Delta\mathrm{t} \\ v_{n+1} &= v_n - \mathrm{i}k\Delta\mathrm{t} p_n \\ p_{n+1} &= p_n - \mathrm{i}kc^2\Delta\mathrm{t}[(1-\beta)v_n + \beta v_{n+1}] \end{aligned}\right\} \,. \tag{76}$$

After some algebraic manipulations and substitutions, the system of equations is

$$\mathbf{z}_{n+1} = \mathbf{A}\mathbf{z}_n \;, \tag{77}$$

where

$$\mathbf{A} := \begin{bmatrix} 1 & \Delta\mathrm{t} & -\mathrm{i}k\Delta\mathrm{t}^2 \\ 0 & 1 & -\mathrm{i}k\Delta\mathrm{t} \\ 0 & -\mathrm{i}kc^2\Delta\mathrm{t} & 1 - \beta k^2 c^2 \Delta\mathrm{t}^2 \end{bmatrix} \,, \tag{78}$$

is the amplification matrix. The characteristic polynomial $f(\lambda)$ of $\mathbf{A}$ is

$$f(\lambda) = (1-\lambda)\left[\lambda^2 + (\beta\Omega^2 - 2)\lambda + (1 + \Omega^2 - \beta\Omega^2)\right] \;, \tag{79}$$

where $\Omega = ck\Delta\mathrm{t}$.

The roots of $f(\lambda)$ (λ such that $f(\lambda) = 0$) are the eigenvalues of $\mathbf{A}$. Note that there is always a single real root $\lambda_3 = 1$. This root corresponds to an eigenvector $[1, 0, 0]^T$. Since λ_3 has no relevant effect on stability, from this point forward it will be ignored. Proceeding forward then, there are two cases of interest:

1. Presto [37] and Dyna [16, 40]: $\beta = 1$: In this case the eigenvalues $\lambda_{1,2}$ are the solutions to the equation

$$\lambda^2 + (\Omega^2 - 2)\lambda + 1 \;=\; 0 \,. \tag{80}$$

This equation has solutions

$$\lambda_{1,2} = \frac{1}{2}\left[2 - \Omega^2 \ \pm \sqrt{(\Omega^2-2)^2 - 4}\,\right] . \tag{81}$$

Assume $\Omega \leqslant 2$. Then $[(\Omega^2-2)^2 - 4] \leqslant 0$ and

$$\lambda_{1,2} = \frac{1}{2}\left[2 - \Omega^2 \ \pm \mathrm{i}\sqrt{4 - (\Omega^2-2)^2}\,\right] . \tag{82}$$

Finally, this implies that

$$\left.\begin{aligned} |\lambda_{1,2}|^2 &= \frac{1}{4}\left[(2-\Omega^2)^2 + 4 - (\Omega^2-2)^2\,\right] \\ &= 1 \end{aligned}\right\} . \tag{83}$$

2. Alegra [25]: $\beta = 1/2$: In this case the eigenvalues $\lambda_{1,2}$ are the solutions to the equation

$$\lambda^2 + \left(\frac{1}{2}\Omega^2 - 2\right)\lambda + \left(1 + \frac{1}{2}\Omega^2\right) \ = \ 0 . \tag{84}$$

This equation has solutions

$$\lambda_{1,2} = \frac{1}{2}\left[\left(2 - \frac{1}{2}\Omega^2\right) \ \pm \Omega\sqrt{\frac{1}{4}\Omega^2 - 4}\,\right] . \tag{85}$$

Assume $\Omega \leqslant 4$. Then $\left(\frac{1}{4}\Omega^2 - 4\right) \leqslant 0$ and

$$\lambda_{1,2} = \frac{1}{2}\left[\left(2 - \frac{1}{2}\Omega^2\right) \ \pm \mathrm{i}\Omega\sqrt{4 - \frac{1}{4}\Omega^2}\,\right] . \tag{86}$$

Finally, this implies that

$$\left.\begin{aligned} |\lambda_{1,2}|^2 &= \frac{1}{4}\left[\left(2 - \frac{1}{2}\Omega^2\right)^2 \ + \ \Omega^2\left(4 - \frac{1}{4}\Omega^2\right)\right] \\ &= \frac{1}{4}\left[4 + 2\Omega^2\right] \\ &= 1 + \frac{1}{2}\Omega^2 \\ &\geqslant 1 \end{aligned}\right\} . \tag{87}$$

Remarks 5.3.

1. When $\beta = 1$, the stability criterion is $\Omega \leqslant 2$. This is consistent with the ODE results of section 4 and is the standard CFL estimate.
2. When $\beta = 1/2$ the algorithm is *unconditionally unstable*.
3. For the fully non-linear problem [25], the choice $\beta = 1/2$ is total-energy conservative but unstable. The choice $\beta = 1$ is conditionally (linearly) stable, but does not conserve total energy. There does not exist a central-difference method that is both conservative and stable. That is one of the primary motivations for considering a midpoint predictor-corrector algorithm.

5.3 Midpoint Predictor-Corrector

The predictor-corrector algorithm can be written as

$$\left.\begin{aligned} u_{n+1}^{(i+1)} &= u_n + v_{n+1/2}^{(i+1)}\Delta\mathrm{t} \\ v_{n+1}^{(i+1)} &= v_n - \mathrm{i}k\Delta\mathrm{t}\,p_{n+1/2}^{(i)} \\ p_{n+1} &= p_n - \mathrm{i}kc^2\Delta\mathrm{t}\,v_{n+1/2}^{(i+1)} \end{aligned}\right\} , \tag{88}$$

where $2(\cdot)_{n+1/2} = (\cdot)_n + (\cdot)_{n+1}$. After some algebraic manipulations and substitutions, the system of equations can be written as

$$\mathbf{z}_{n+1}^{(i+1)} = \mathbf{B}_0 \mathbf{z}_n + \mathbf{B}_1 \mathbf{z}_{n+1}^{(i)} + \mathbf{B}_2 \mathbf{z}_{n+1}^{(i+1)} \ , \tag{89}$$

where

$$\mathbf{B}_0 := \begin{bmatrix} 1 & \frac{1}{2}\Delta\mathrm{t} & 0 \\ 0 & 1 & -\frac{1}{2}\mathrm{i}k\Delta\mathrm{t} \\ 0 & -\frac{1}{2}\mathrm{i}kc^2\Delta\mathrm{t} & 1 \end{bmatrix} \ , \tag{90}$$

$$\mathbf{B}_1 := \begin{bmatrix} 0 & 0 & 0 \\ 0 & 0 & -\frac{1}{2}\mathrm{i}k\Delta\mathrm{t} \\ 0 & 0 & 0 \end{bmatrix} \ , \tag{91}$$

and

$$\mathbf{B}_2 := \begin{bmatrix} 0 & \frac{1}{2}\Delta\mathrm{t} & 0 \\ 0 & 0 & 0 \\ 0 & -\frac{1}{2}\mathrm{i}kc^2\Delta\mathrm{t} & 0 \end{bmatrix} \ . \tag{92}$$

Some simple algebra yields

$$\mathbf{z}_{n+1}^{(i+1)} = \mathbf{A}_0 \mathbf{z}_n + \mathbf{A}_1 \mathbf{z}_n^{(i)} \ , \tag{93}$$

where

$$\mathbf{A}_0 = [\mathbf{I} - \mathbf{B}_2]^{-1} \mathbf{B}_0 \ , \tag{94}$$

and

$$\mathbf{A}_1 = [\mathbf{I} - \mathbf{B}_2]^{-1} \mathbf{B}_1 \ . \tag{95}$$

As in section 4, the final amplification matrix is

$$\mathbf{A} = [\mathbf{A}_0 + \mathbf{A}_1 (\mathbf{A}_0 + \mathbf{A}_1)] \ . \tag{96}$$

Remarks 5.4.

1. The matrix $[\mathbf{I} - \mathbf{B}_2]$ is always non-singular. In fact, $\det[\mathbf{I} - \mathbf{B}_2] = 1$.
2. Once again, it can be shown analytically, and verified numerically, that the eigenvalues of $\mathbf{A}$ depend only upon the dimensionless quantity $\Omega = ck\Delta\mathrm{t}$. The algebraic details, being somewhat tedious, are omitted.
3. For general partial differential equation finite-difference schemes in both space and time, the amplification matrix $\mathbf{A}$ is a function of the time step $\Delta\mathrm{t}$ and the wavenumber k [30].

Once again MATLAB® ™is used to numerically calculate the amplification matrix $\mathbf{A}$ and extract the eigenvalues. The plots in this section are generated with that software package. Figure 7 is a plot of the eigenvalues of $\mathbf{A}$ versus Ω. As for the central difference method, there is always a single real eigenvalue equal to 1.

Remarks 5.5.

1. The stability requirement is $\Omega \leqslant 2$, the same as in section 4.
2. If only one iteration of the predictor-corrector algorithm is done, then

$$\left.\begin{aligned} u_{n+1} &= u_n + \frac{1}{2}\Delta\mathrm{t}(v_n + v_{n+1}) \\ v_{n+1} &= v_n - \mathrm{i}k\Delta\mathrm{t}p_n \\ p_{n+1} &= p_n - \frac{1}{2}\mathrm{i}kc^2\Delta\mathrm{t}(v_n + v_{n+1}) \end{aligned}\right\} \ .$$

   Note that the velocity and pressure update equations are the same as for the central-difference method with $\beta = 1/2$ (see equation (76)). The difference in the position update equation has no effect on stability; only the second two slots of the first row of $\mathbf{A}$ in equation (78) change, which does not change the eigenvalues of $\mathbf{A}$. Thus the predictor-corrector algorithm is unconditionally unstable if only one iteration is computed. At least two iterations must be performed to recover (conditional) stability. As in section 4, using *three iterations results in an unconditonally unstable* algorithm.

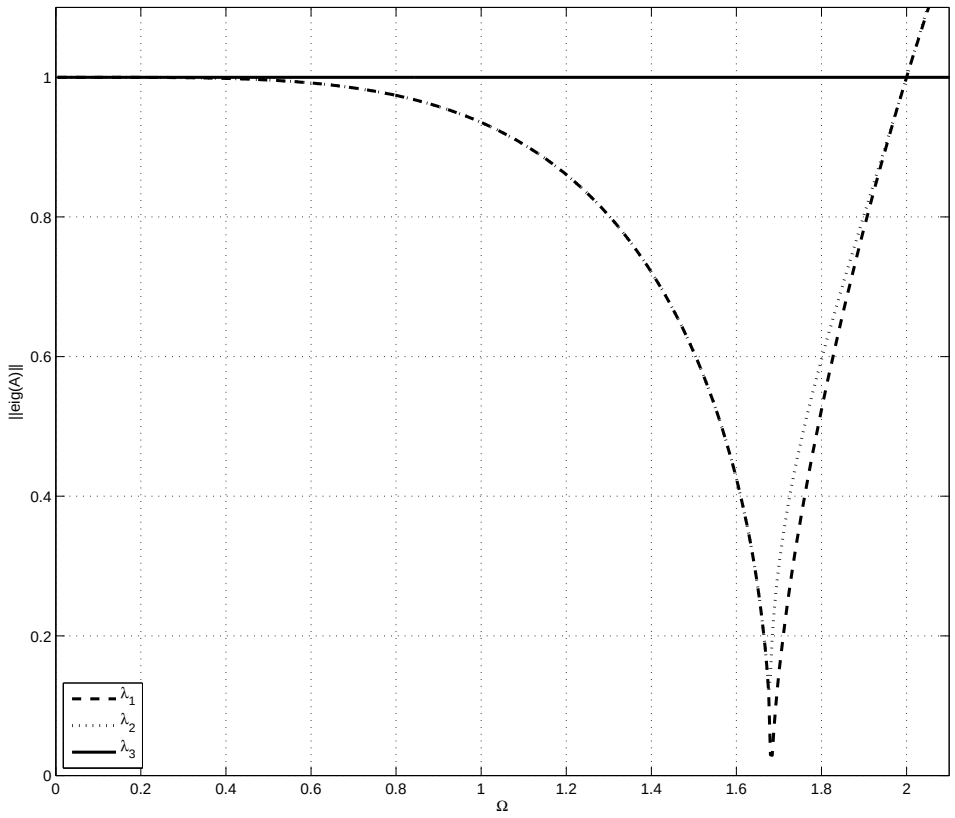

Figure 7. Modulus of the eigenvalues of $\mathbf{A}$ versus Ω.

3. For the fully non-linear problem, the midpoint predictor-corrector algorithm is both (linearly) stable and total-energy conservative [32, 33].

5.4 Convergence Criteria

Consider numerically solving the system of equations (72) on the closed time interval $[0, T]$, with time step $\Delta t = T/N$ for some integer $N > 0$, using any of the time integration schemes outlined in this report. Note that $\Delta t \searrow 0$ as $N \nearrow \infty$. In general, all the schemes have the form

$$\mathbf{z}_{n+1} = \mathbf{A}\mathbf{z}_n \ , \tag{97}$$

where $\mathbf{A}$ is the algorithmic amplification matrix. The *Lax Equivalence Theorem* [30, 36] details the sufficient conditions for which the numerical algorithm is convergent. In particular, linear growth is allowed in the sense that[1]

$$\exists\, M \geqslant 0 \text{ and } \exists\, \tau > 0 \quad \text{such that} \quad \|\mathbf{A}\| \leqslant 1 + M\Delta t \quad \forall\, \Delta t \in [0, \tau) \ . \tag{98}$$

This is motivated by the fact that

$$\left\|\mathbf{A}^N\right\| \leqslant \|\mathbf{A}\|^N \leqslant (1 + M\Delta t)^N = \left(1 + \frac{MT}{N}\right)^N \leqslant \exp(MT) \quad \forall\, N > (T/\tau) \ , \tag{99}$$

[1] In this sub-section, M denotes a fixed constant greater than or equal to zero. It may not be the same in all equations.

so that $\left\|\mathbf{A}^N\right\|$ is uniformly bounded as $N \nearrow \infty$, or equivalently, as $\Delta t \searrow 0$.

For all the (unstable) methods discussed here, one can write (for $\Omega \ll 1$)

$$\rho(\mathbf{A}) \leqslant 1 + K\Omega^L \,, \tag{100}$$

with $K > 0$ and $L \geqslant 1$. Since $\rho(\mathbf{A}) \leqslant \|\mathbf{A}\|$, the linear growth bound (98) requires that

$$\exists\, M \geqslant 0 \quad \text{such that} \quad \rho(\mathbf{A}) \leqslant 1 + M\Delta t \,. \tag{101}$$

Recalling that $\Omega_{\max} = 2c(\Delta t/h)$, a sufficient condition for the immediately preceding inequality to hold is that

$$\exists\, M \geqslant 0 \quad \text{such that} \quad \left(2c\frac{\Delta t}{h}\right)^L \leqslant M^{(L-1)}\Delta t \,. \tag{102}$$

This is equivalent to

$$\Delta t \leqslant M\left(\frac{h}{2c}\right)^{L/(L-1)} \quad \Longleftrightarrow \quad \Delta t \propto h^{L/(L-1)} \,. \tag{103}$$

There are two cases of interest:

1. Central-Difference with $\beta = 1/2$: In this case $L = 2$ and thus
$$\Delta t \leqslant M\left(\frac{h}{2c}\right)^2 \quad \Longleftrightarrow \quad \Delta t \propto h^2 \,.$$
2. Midpoint predictor-corrector with three iterations: In this case $L = 6$ and thus
$$\Delta t \leqslant M\left(\frac{h}{2c}\right)^{(6/5)} \quad \Longleftrightarrow \quad \Delta t \propto h^{(6/5)} \,.$$

Remarks 5.6.

1. The unstable methods may converge as $\{h, \Delta t\} \searrow 0$ if the time step Δt goes to zero fast enough, and generally faster than h goes to zero, so that $(\Delta t/h) \searrow 0$. This may be undesirable, as it (perhaps significantly) increases computational cost relative to the case where $\Delta t \propto h$.
2. If, as the mesh is refined, $(\Delta t/h) \searrow 0$, then also $\Omega_{\max} \searrow 0$. Thus eventually $\Omega_{\max}$ will be small enough that the asymptotic expansion of equation (100) is valid.
3. The bound (98) implies the bound (101), but not conversely. Thus while (101) is necessary for convergence (it is the vonNeumann necessary condition [30, section 4.7]), it may not be sufficient. The bound (98) is sufficient for convergence.

5.5 A Simplified Time-Step Estimate

Recall from section 4.1 that the stable time step may be estimated as

$$\Delta t \leq \frac{1}{2}\Omega_{\text{crit}}\frac{h}{c} \,, \tag{104}$$

where $\Omega_{\text{crit}} = 2\left(\sqrt{1+\xi^2} - \xi\right)$. For large $\xi \gg 1$, this is approximately $\Omega_{\text{crit}} \approx \xi^{-1}$. Substituting this into the above produces the approximation

$$\left.\begin{aligned} \Delta t &\leqslant \frac{1}{2}\Omega_{\text{crit}}\frac{h}{c} \\ &\approx \frac{1}{2\xi_{\max}} \cdot \frac{h}{c} \\ &= \frac{1}{2c_1 + 2c_2\frac{h}{c}|\nabla\cdot\mathbf{v}|} \cdot \frac{h}{c} \\ &= \frac{h}{2c_1 c + 2c_2 h|\nabla\cdot\mathbf{v}|} \end{aligned}\right\} \,. \tag{105}$$

Next, assume that $2c_1 \leqslant 1$ and define

$$\tilde{c} := c + 2c_2 h|\nabla \cdot \mathbf{v}| \quad \geqslant \; 2c_1 c + 2c_2 h|\nabla \cdot \mathbf{v}| \; . \tag{106}$$

This finally yields the approximate time step estimate

$$\Delta \mathrm{t} \lesssim \frac{h}{\tilde{c}} \; . \tag{107}$$

Notice that $\tilde{c} \geqslant c$ can be interpreted as a prediction of the sound speed based upon the dissipative effects of the artificial viscosity.

6 vonNeumann Stability Analysis

In an effort to fully justify the analyses of the preceding section(s), once again consider the linearized hyperbolic system

$$\frac{\mathrm{d}}{\mathrm{dt}} \begin{bmatrix} u \\ v \\ p \end{bmatrix} = \begin{bmatrix} v \\ -p_x + \nu v_{xx} \\ -c^2 v_x \end{bmatrix} \; . \tag{108}$$

Let the displacement field and velocity field be node-centered and let the pressure field be cell-centered. This is a *staggered grid* [5, 6] spatial discretization. A standard lumped mass finite element (or finite difference) discretization of this system of equations yields the difference stencil

$$\left.\begin{aligned} \frac{\mathrm{d}}{\mathrm{dt}} u(x_j, \mathrm{t}) &= v(x_j, \mathrm{t}) \\ \frac{\mathrm{d}}{\mathrm{dt}} v(x_j, \mathrm{t}) &= -\frac{1}{h}[p(x_{j+1/2}, \mathrm{t}) - p(x_{j-1/2}, \mathrm{t})] + \frac{\nu}{h^2}[v(x_{j+1}, \mathrm{t}) - 2v(x_j, \mathrm{t}) + v(x_{j-1}, \mathrm{t})] \\ \frac{\mathrm{d}}{\mathrm{dt}} p\left(x_{j+1/2}, \mathrm{t}\right) &= -\frac{c^2}{h}[v(x_{j+1}, \mathrm{t}) - v(x_j, \mathrm{t})] \end{aligned}\right\} , \tag{109}$$

where $x_{j\pm\beta} := (j \pm \beta)h$ for spatial node index j and $\beta \in [0, 1]$.

Towards the goal of a vonNeumann stability analysis [30, 36], assume all fields have a harmonic spatial variation such that

$$\left.\begin{aligned} u(x_j, \mathrm{t}) &= \exp[\mathrm{i}kjh] \cdot u(\mathrm{t}) \\ v(x_j, \mathrm{t}) &= \exp[\mathrm{i}kjh] \cdot v(\mathrm{t}) \\ p\left(x_{j+1/2}, \mathrm{t}\right) &= \exp\left[\mathrm{i}k(j + 1/2)h\right] \cdot p(\mathrm{t}) \end{aligned}\right\} , \tag{110}$$

where $k \geqslant 0$ is the spatial wavenumber. For notational convenience define

$$\theta := k\, h \; \geqslant 0 \; .$$

After some algebraic manipulations and trigonometric expansions, again using MATHEMATICA ® ™, this reduces the system of equations (109) to the ordinary differential equations

$$\frac{\mathrm{d}}{\mathrm{dt}} \begin{bmatrix} u \\ v \\ p \end{bmatrix} = \underbrace{\begin{bmatrix} 0 & 1 & 0 \\ 0 & a_{vv} & a_{vp} \\ 0 & a_{pv} & 0 \end{bmatrix}}_{\mathbf{A}^h} \begin{bmatrix} u \\ v \\ p \end{bmatrix} \; , \tag{111}$$

where

$$a_{vv} = \frac{\nu}{h^2}(-2 + 2\cos\theta) \; , \tag{112}$$

$$a_{vp} = -\frac{1}{h} 2\,\mathrm{i}\, \sin\left(\frac{\theta}{2}\right) \; , \tag{113}$$

and

$$a_{pv} = -\frac{1}{h} 2\,\mathrm{i}\, c^2 \sin\left(\frac{\theta}{2}\right) \; . \tag{114}$$

Remarks 6.1.

1. The exact solution of (111) is $\mathbf{z}(\mathrm{t}) = \exp[\mathrm{t} \cdot \mathbf{A}^h]\, \mathbf{z}(0)$, where $\mathbf{z} = [u, v, p]^T$.

2. The eigenvalues of the matrix $\mathbf{A}^h$ can be used to evaluate the analytic dispersion relationship for the spatial discretization itself. When $\nu = 0$ the eigenvalues of $\mathbf{A}^h$ are

$$\lambda^h := \left\{ 0, -\frac{2\,\mathrm{i}\,c}{h} \sin\left(\frac{kh}{2}\right), \frac{2\,\mathrm{i}\,c}{h} \sin\left(\frac{kh}{2}\right) \right\} .$$

   The exact dispersion relationship for the wave equation is $\lambda = \mathrm{i}\,c\,k$. The relative dispersion error is thus

$$\frac{\lambda^h}{\lambda} = \frac{2}{kh} \sin\left(\frac{kh}{2}\right) \approx 1 - \frac{k^2h^2}{24} + \frac{k^4h^4}{1920} + \mathcal{O}(kh)^6 .$$

   The (lumped mass) spatial discretization causes waves with high spatial frequency (large wavenumber) to travel more slowly (for $h \ll 1$) [17, 21, 27, 31].

At this point it is straight-forward to apply a time integration algorithm to the system of ordinary differential equations (111). Let $\mathbf{z} := [v, p]^T$. The displacement update equation is omitted since it always yields an amplification eigenvalue of 1 with corresponding eigenvector $[1, 0, 0]^T$.

1. Alegra central-difference:

$$\mathbf{z}_{n+1} = \begin{bmatrix} 1 + a_{vv}\Delta\mathrm{t} & a_{vp}\Delta\mathrm{t} \\ \frac{1}{2}a_{pv}\Delta\mathrm{t} & 1 \end{bmatrix} \mathbf{z}_n + \begin{bmatrix} 0 & 0 \\ \frac{1}{2}a_{pv}\Delta\mathrm{t} & 0 \end{bmatrix} \mathbf{z}_{n+1} . \tag{115}$$

2. Presto central-difference:

$$\mathbf{z}_{n+1} = \begin{bmatrix} 1 + a_{vv}\Delta\mathrm{t} & a_{vp}\Delta\mathrm{t} \\ 0 & 1 \end{bmatrix} \mathbf{z}_n + \begin{bmatrix} 0 & 0 \\ a_{pv}\Delta\mathrm{t} & 0 \end{bmatrix} \mathbf{z}_{n+1} . \tag{116}$$

3. Midpoint predictor-corrector: for iteration index (i),

$$\mathbf{z}_{n+1}^{(i+1)} = \mathbf{B}_0\mathbf{z}_n + \mathbf{B}_1\mathbf{z}_{n+1}^{(i)} + \mathbf{B}_2\mathbf{z}_{n+1}^{(i+1)} , \tag{117}$$

   where

$$\mathbf{B}_0 := \begin{bmatrix} 1 + \frac{1}{2}a_{vv}\Delta\mathrm{t} & \frac{1}{2}a_{vp}\Delta t \\ \frac{1}{2}a_{pv}\Delta\mathrm{t} & 1 \end{bmatrix} , \tag{118}$$

$$\mathbf{B}_1 := \begin{bmatrix} \frac{1}{2}a_{vv}\Delta\mathrm{t} & \frac{1}{2}a_{vp}\Delta\mathrm{t} \\ 0 & 0 \end{bmatrix} , \tag{119}$$

   and

$$\mathbf{B}_2 := \begin{bmatrix} 0 & 0 \\ \frac{1}{2}a_{pv}\Delta\mathrm{t} & 0 \end{bmatrix} . \tag{120}$$

Using the same algebraic manipulations as in the previous section(s) of this report, an algorithmic amplification matrix can be derived for each time integrator. The eigenvalues of that matrix depend on the non-dimensional parameters $\theta \geqslant 0$, CFL number

$$\Phi := \frac{c\,\Delta\mathrm{t}}{h} \geqslant 0 ,$$

and dimensionless damping ratio

$$\xi := \frac{\nu}{c\,h} \geqslant 0 .$$

The details are omitted in an effort to be concise and not be redundant.

6.1 Truncation Error

Consider the simplified case of no physical viscosity where $\nu = 0 \iff \xi = 0$. For a wavenumber $k \geqslant 0$, the exact solution (in Fourier phase space) over a time interval $\Delta\mathrm{t} \geqslant 0$ is

$$\exp[\mathrm{i}\,\omega\Delta\mathrm{t}] = \exp[\mathrm{i}\,ck\Delta\mathrm{t}] = \exp[\mathrm{i}\,c\,\Delta\mathrm{t}\,h^{-1}\cdot kh] = \exp[\mathrm{i}\,\Phi\,\theta] \; .$$

Thus the order of accuracy, or equivalently, the truncation error, of a numerical method can be determined by examining the difference

$$\mathrm{LTE} := \left(\bar{\lambda}^h - \exp[\mathrm{i}\,\Phi\,\theta]\right) \; , \tag{121}$$

where $\bar{\lambda}^h \in \mathbb{C}$ is a (possibly complex) eigenvalue of the numerical amplification matrix.

1. Alegra central difference:

   $$\mathrm{LTE} = \frac{1}{4}\Phi^2\theta^2 \; + \; \mathcal{O}(\theta^3) \; .$$

   The Alegra central-difference method is globally first-order accurate.

2. Presto central difference:

   $$\mathrm{LTE} = \frac{1}{24}\mathrm{i}\,\Phi(\Phi^2 - 1)\theta^3 \; + \; \mathcal{O}(\theta^4) \; .$$

   The Presto central-difference method is globally second-order accurate.

3. Midpoint predictor-corrector: For one iteration,

   $$\mathrm{LTE} = \frac{1}{4}\Phi^2\theta^2 \; + \; \mathcal{O}(\theta^3) \; ,$$

   which yields global first-order accuracy. For two or more iterations,

   $$\mathrm{LTE} = -\frac{1}{24}\mathrm{i}\,\Phi(\Phi + 2\Phi^3)\theta^3 \; + \; \mathcal{O}(\theta^4) \; ,$$

   which yields global second-order accuracy.

6.2 Amplification and Phase

Additionally, as in section 4.2, the relative phase error can be computed as

$$\text{Relative phase error} = \frac{\Delta\mathrm{t}^{-1}\arg(\bar{\lambda}^h)}{c\,k} \; = \; \frac{\arg(\bar{\lambda}^h)}{c\,k\,\Delta\mathrm{t}} \; = \; \frac{\arg(\bar{\lambda}^h)}{\Phi\,k\,h} \; = \; \frac{\arg(\bar{\lambda}^h)}{\Phi\,\theta} \; .$$

Again consider the simplified case of no physical viscosity where $\nu = 0 \iff \xi = 0$.

1. Alegra central-difference: Figure 8 plots the modulus of the eigenvalues of the amplification matrix versus Φ and θ for the Alegra central-difference algorithm. When $\theta = \pi$ the eigenvalues of the amplification matrix are

   $$\lambda = 1 - \Phi^2 \; \pm \; \mathrm{i}\,\Phi\sqrt{4 - \Phi^2} \; . \tag{122}$$

   These have modulus

   $$|\lambda|^2 = 1 + 2\,\Phi^2 \geqslant 1 \; . \tag{123}$$

2. Presto central-difference: Figure 9 plots the modulus of the eigenvalues of the amplification matrix versus Φ and θ for the Presto central-difference algorithm. The eigenvalues have modulus 1 for $\Phi \leqslant 1$. Figure 10 shows the relative phase error for the Presto central-difference algorithm. When $\Phi = 1$, the relative phase error is 1 for all θ, i.e., the phase is exact. This is a well known result [17, 18, 31].

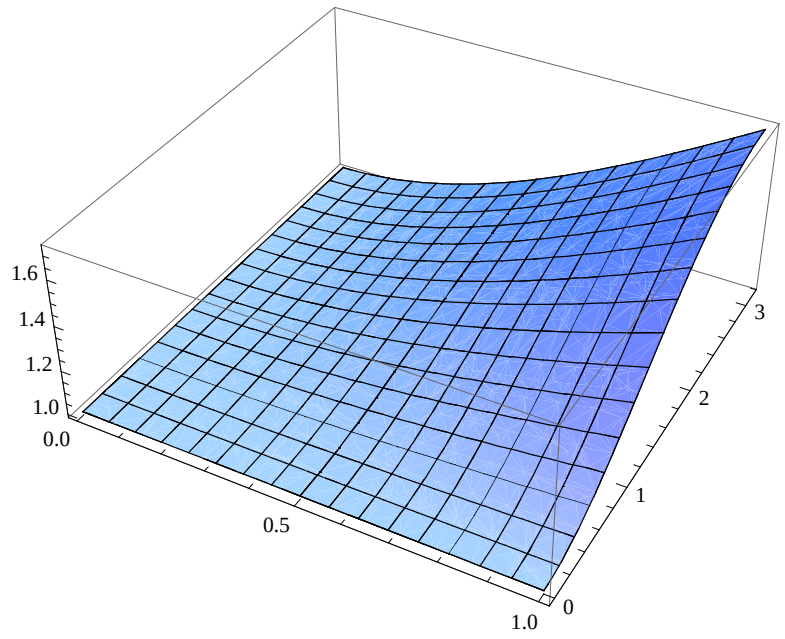

Figure 8. Modulus of the eigenvalues of the amplification matrix for the ALEGRA central-difference algorithm. Plot axes are $0 \leqslant \Phi \leqslant 1$ and $0 \leqslant \theta \leqslant \pi$.

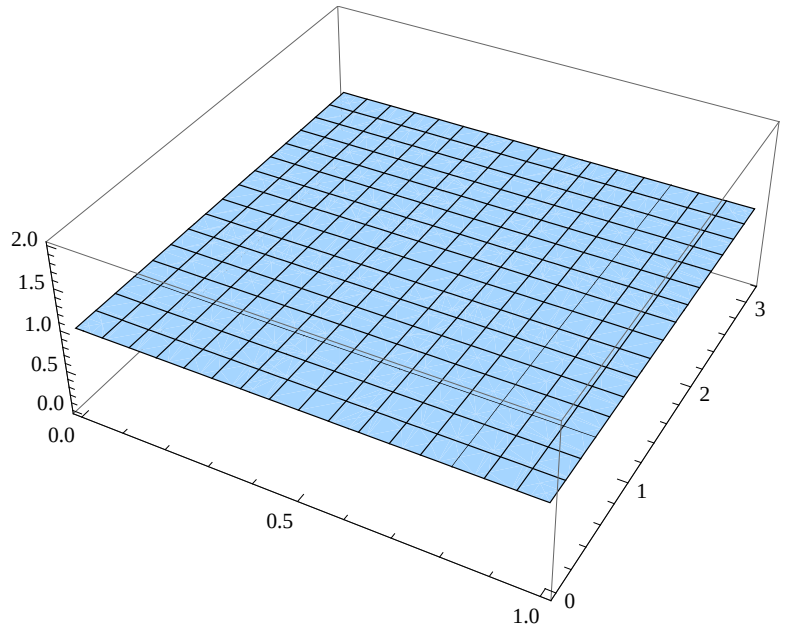

Figure 9. Modulus of the eigenvalues of the amplification matrix for the PRESTO central-difference algorithm. Plot axes are $0 \leqslant \Phi \leqslant 1$ and $0 \leqslant \theta \leqslant \pi$.

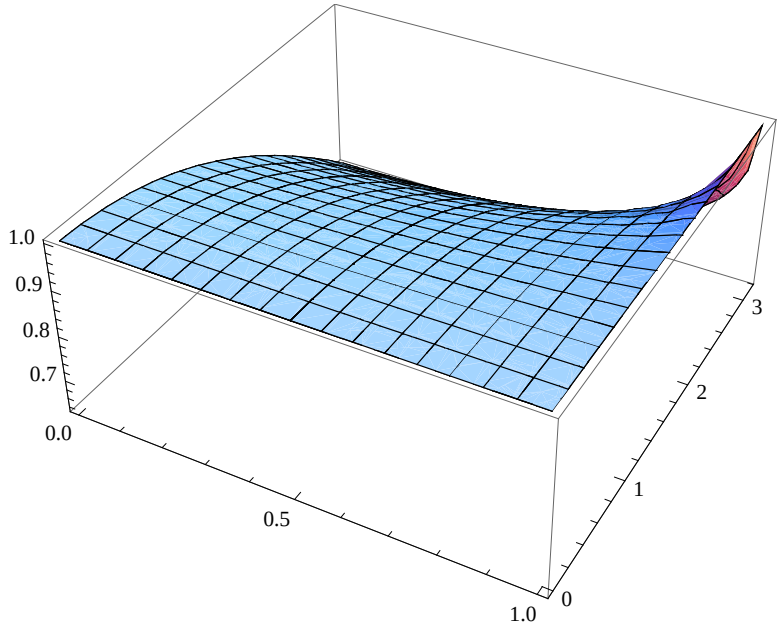

Figure 10. Relative phase error for the PRESTO central-difference algorithm. Plot axes are $0 \leqslant \Phi \leqslant 1$ and $0 \leqslant \theta \leqslant \pi$.

3. Midpoint predictor-corrector: Figure 11 plots the modulus of the eigenvalues of the amplification matrix versus Φ and θ for the midpoint predictor-corrector algorithm. Plots are shown for two, three and four iterations. Assume again that $\theta = \pi$. For the three iteration case the eigenvalues of the amplification matrix are

$$\lambda = 1 - 2\Phi^2 + 2\Phi^4 - \Phi^6 \ \pm \ \mathrm{i}\,\Phi\sqrt{4 - 8\Phi^2 + 12\Phi^4 - 8\Phi^6 + 4\Phi^8 - \Phi^{10}}\,. \tag{124}$$

These have modulus

$$|\lambda|^2 = 1 + 2\,\Phi^6 \geqslant 1\,. \tag{125}$$

Figure 12 shows the relative phase error for the midpoint predictor-corrector algorithm with two iterations. The relative phase error is less than 1 for all $\Phi > 0$ and for all $\theta > 0$. The combined space and time discretization causes waves with high spatial frequency (large wavenumber) to travel more slowly. For the fully non-linear problem an oscillatory wavetrain may be observed behind a shock. The relative phase error for the four iteration case is very similar to that of the two iteration case and thus is omitted.

Remarks 6.2.

1. The relative phase error is not shown for the unstable algorithms.
2. The amplification matrix eigenvalues can also be calculated as a function of θ, Φ and the non-dimensional parameter

$$\kappa := \frac{\nu \Delta \mathrm{t}}{h^2}\,.$$

However, noting that $\kappa = \Phi\,\xi$, the choice of using ξ or κ is simply a matter of convenience or personal preference.

3. The ALEGRA central-difference algorithm is unconditionally unstable.
4. The PRESTO central-difference algorithm is stable when $\Phi \leqslant 1$. This is the expected result.
5. The midpoint predictor-corrector is stable for two and four iterations when $\Phi \leqslant 1$. For three iterations it is unconditionally unstable.

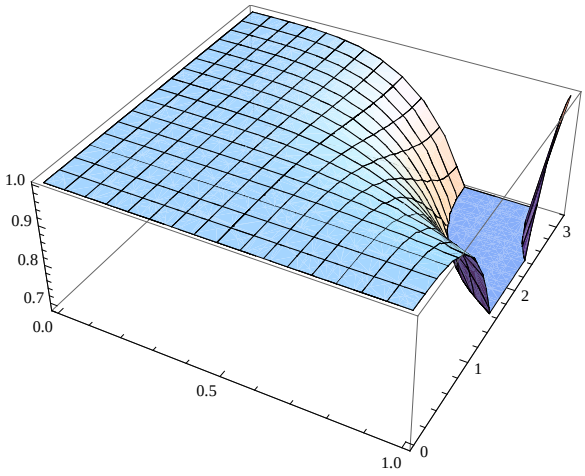

(a) Two Iterations

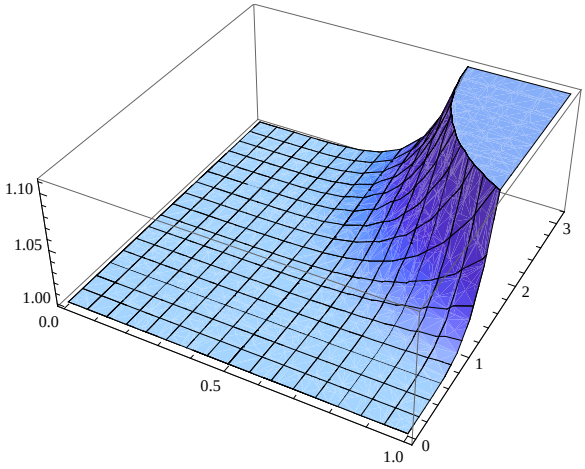

(b) Three Iterations

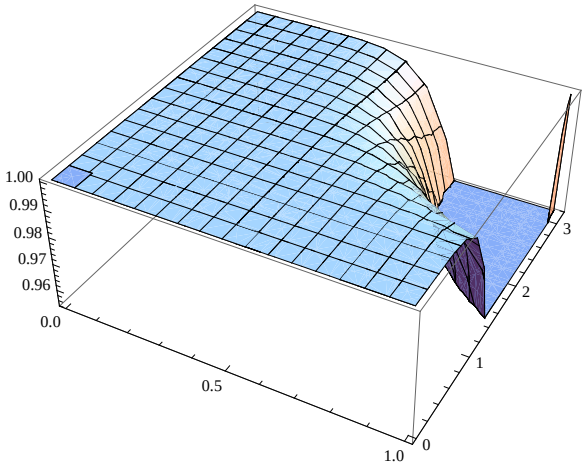

(c) Four Iterations

Figure 11. Modulus of the eigenvalues of the amplification matrix for the midpoint predictor-corrector algorithm. Plot axes are $0 \leqslant \Phi \leqslant 1$ and $0 \leqslant \theta \leqslant \pi$. Shown are the two, three, and four iteration cases.

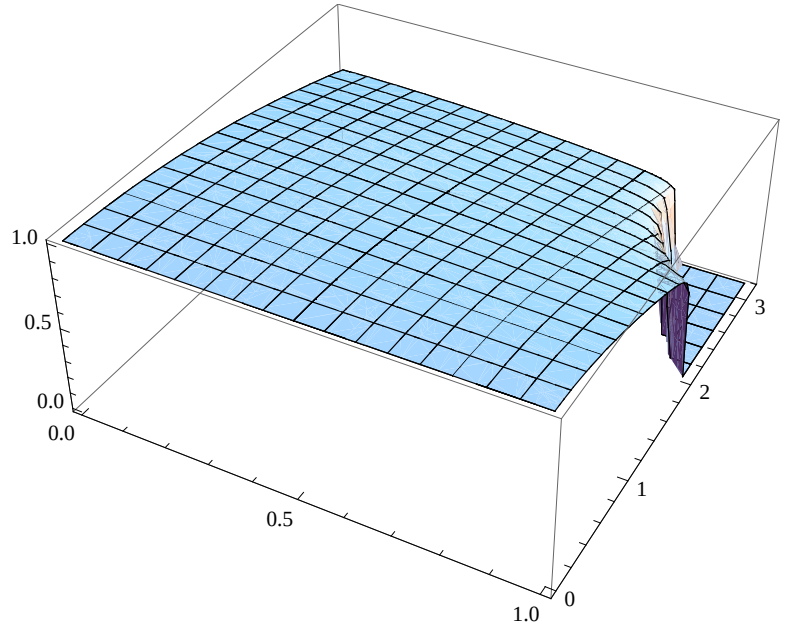

Figure 12. Relative phase error for the midpoint predictor-corrector algorithm with two iterations. Plot axes are $0 \leqslant \Phi \leqslant 1$ and $0 \leqslant \theta \leqslant \pi$.

6. Consider the PRESTO central-difference algorithm, or the midpoint predictor-corrector algorithm with an even number of iterations. For those time integration schemes, when $\theta = \pi$, the relevant non-complex positive eigenvalue of the amplification matrix equals $+1$ when

$$\Phi = \left(\sqrt{1 + \xi^2} - \xi \right) .$$

   This is of course the expected result. The details of the MATHEMATICA® $^{\text{TM}}$analysis are omitted.

7. The analysis of this section confirms that the simplified analyses of the previous section(s) are in fact both correct and highly useful.

7 Numerical Simulations

Unless otherwise indicated, for all numerical simulations the stable time step is estimated as

$$\Delta \mathrm{t} = CFL \ \cdot \ \min(\Delta \mathrm{t}_1, \Delta \mathrm{t}_2) \ ,$$

where $CFL \leqslant 1$ is a scaling factor. The possible time steps are defined as

$$\Delta \mathrm{t}_1 := \frac{h}{c + 2c_2 h |\nabla \cdot \mathbf{v}|} \ ,$$

and

$$\Delta \mathrm{t}_2 := \frac{h}{c \left(\sqrt{1 + \xi_{\max}^2} + \xi_{\max} \right)} \ ,$$

with $\xi_{\max} = c_1 + c_2 h c^{-1} |\nabla \cdot \mathbf{v}|$. The parameter $h > 0$ is an element characteristic length scale determined from the volume and the strain-gradient operator(s), described in [38, section 3.5], and based upon the analysis in [12]. The minimum time step over all elements is chosen.

7.1 Periodic Breaking Wave

As a numerical test of the midpoint predictor-corrector algorithm, consider a simple periodic breaking wave problem similar to the one described in [7, 8]. In one dimension the domain of the problem is $[0, 1]$. The material is a gamma-law ideal gas [26] with $\gamma = 5/3$. The initial density has a sinusoidal variation

$$\rho(x, 0) = 0.001 \left[1.0 + 0.1 \sin(2\pi x)\right] .$$

The initial pressure is

$$p(x, 0) = 10^6 \left[\frac{\rho(x, 0)}{0.001}\right]^{\gamma} ,$$

and the initial velocity is

$$v(x, 0) = 2\frac{(c_{s0} - c_s)}{\gamma - 1} ,$$

where

$$c_s = \left[\gamma \frac{p(x, 0)}{\rho(x, 0)}\right]^{1/2} ,$$

and

$$c_{s0} = \left[\gamma \frac{10^6}{0.001}\right]^{1/2} .$$

Periodic boundary conditions are applied at coordinates $x = 0$ and $x = 1$. The solution is smooth for a finite time $0 < T_{\text{break}} < \infty$, at which point the wave breaks and a shock forms [7, 8].

The problem is run purely Lagrangian in two-dimensions on the domain $[0, 1] \times [-0.5, 0.5]$ using a 100×1 mesh of Q1/P0 finite elements. The algorithm is described in detail in [32, 33]. The 100 elements are all in a single line along the $x-$axis. Boundary conditions are applied to prevent motion in the $y-$ direction; hourglass modes [2] are not active. The linear artificial viscosity coefficient is chosen $c_1 = 0.15$. The quadratic artificial viscosity coefficient is chosen $c_2 = 2.0$. Figure 13 plots the numerical results of density versus spatial position for different number of fixed point iterations. All plots are at time 3.728×10^{-05}. All simulations are run using a constant $CFL = 0.90$.

Remarks 7.1.

1. Consistent with the preceding analysis, an odd number of iterations generally produces (mildly) unstable results. An even number of iterations appears to be stable.

2. Notice also that the fixed-point iteration appears to converge with an increasing number of iterations to a stable solution. The solution with 7 iterations appears satisfactory, while those with 3 and 5 iterations are somewhat noisy.

7.2 Interacting Blast Waves

As a second numerical test, consider the Woodward-Colella interacting shock wave test problem [41]. In one dimension the domain of the problem is $[0, 1]$. The material is a gamma-law ideal gas with $\gamma = 1.4$. The gas is initially at rest between reflecting walls, with a uniform initial density everywhere equal to 1. On the subdomain $[0, 0.1]$ the initial pressure is 1000 and on the subdomain $[0.9, 1.0]$ the initial pressure is 100. Everywhere else the pressure is initialized to 0.01. Two strong shock waves develop and interact.

The problem is run purely Lagrangian using 400 originally cubic Q1/P0 finite elements. The 400 elements are all in a single line along the $x-$axis. Boundary conditions are applied to prevent motion in the $y-$ and $z-$ directions; hourglass modes are not active. The linear artificial viscosity coefficient is chosen $c_1 = 0.15$. The quadratic artificial viscosity coefficient is chosen $c_2 = 2.0$. Figure 14 plots the numerical results of density versus position for various values of the CFL control parameter. Two fixed-point iterations are used for these simulations.

Remarks 7.2.

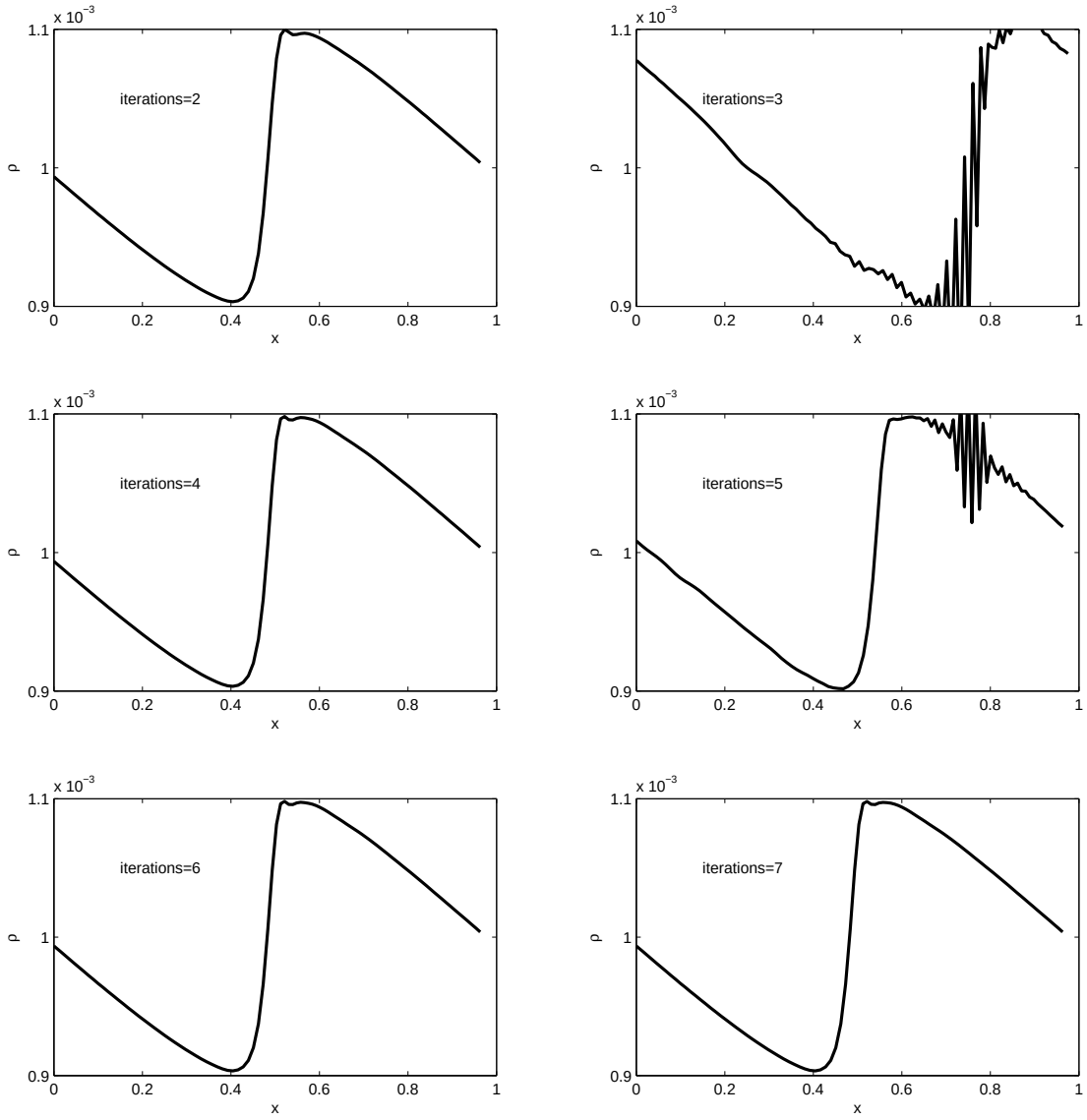

Figure 13. Density versus spatial position for the periodic breaking wave test problem for different number of fixed point iterations. All plots are at time 3.728×10^{-05}. CFL is constant at 0.90.

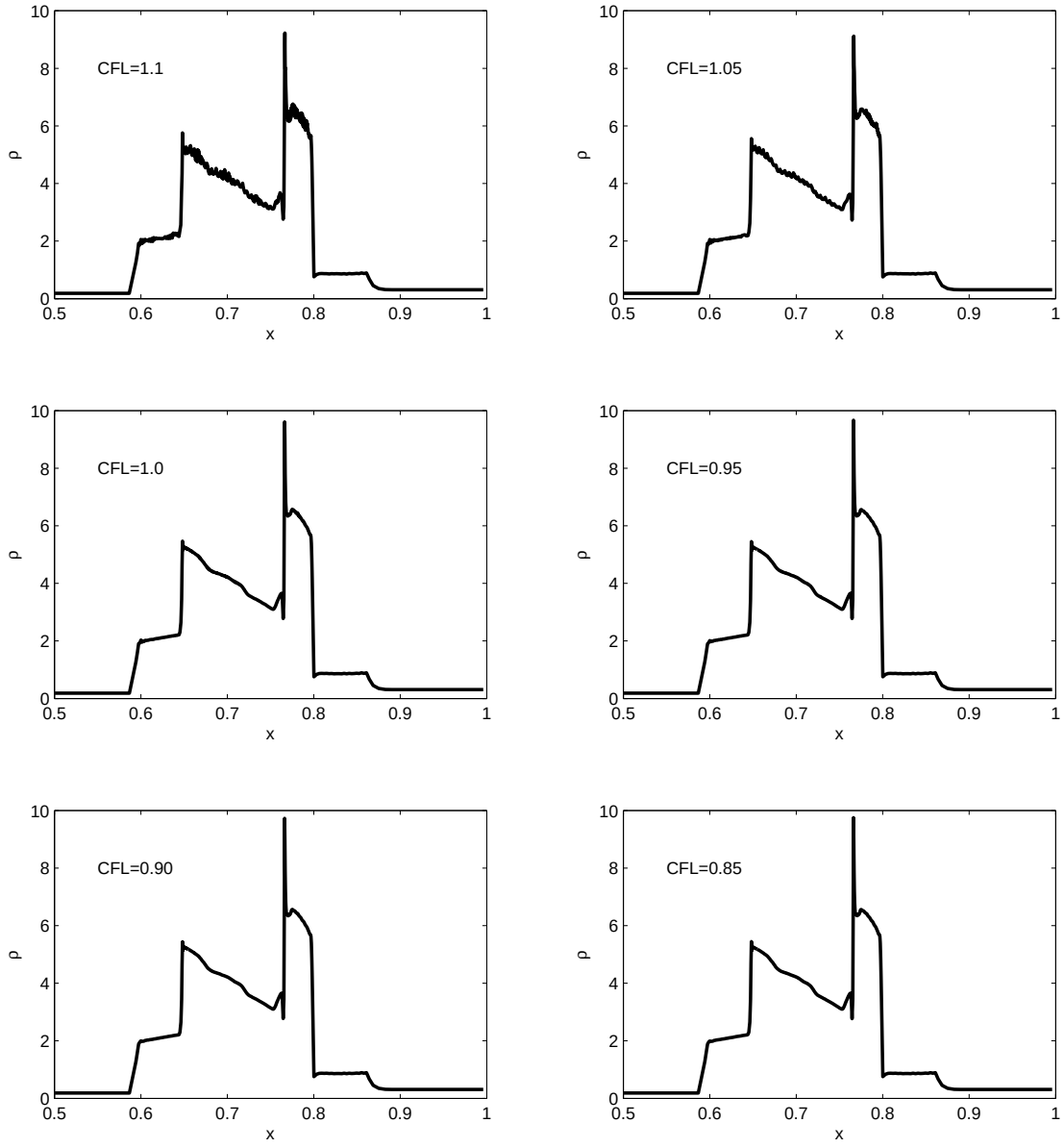

Figure 14. Density versus spatial position for the Woodward-Colella test problem for incrementally decreasing values of the CFL parameter. Plots are at the final time of 0.038.

1. The simulations with $CFL \leqslant 1$ show little if any instability, while the simulations with $CFL > 1$ appear mildly unstable. The time step stability estimate seems to be accurate to within about 5%, at least for this test problem.

2. The large spurious overshoot in density at $x \approx 0.765$ is typical of Lagrangian simulations of this test [24, 29], and does not represent a problem with the time integration algorithm.

8 Closure

This paper has presented an analysis of the algorithmic properties of a midpoint predictor-corrector time integrator for Lagrangian shock hydrodynamics. In particular, the conservation and stability properties of the algorithm have been discussed. Angular momentum conservation and incremental objectivity are achieved in the limit case of an infinite number of iterations. In the case of a finite number of iterations, the errors are limited only by the number of iterations performed. The algorithm does not yield stable solutions in the case of an odd number of iterations. An even number of iterations produces stable results. A discussion of alternative time-stepping algorithms currently used in many codes was included for completeness

---

Acknowledgment: The authors wish to thank Dr. Allen C. Robinson and Dr. Randall M. Summers for their continuing support and encouragement. The authors thank Dr. John H. Carpenter, Dr. Curtis C. Ober, Dr. Thomas E. Voth, Dr. V. Gregory Weirs and Dr. Michael K. Wong for helpful discussions. Dr. Carpenter and Dr. Voth also kindly reviewed initial drafts of this work.

End Note: Many of the technical reports referenced in this paper are available electronically on the web site `www.osti.gov`.

References

[1] Martha L. Abell and James P. Braselton. *Mathematica by Example*. Academic Press, 4th edition, September 2008.

[2] Ted Belytschko and Lee P. Bindeman. Assumed strain stabilization of the eight node hexahedral element. *Computer Methods in Applied Mechanics and Engineering*, **105**(2):225–260, June 1993.

[3] Ted Belytschko, Wing Kam Liu, and Brain Moran. *Nonlinear Finite Elements for Continua and Structures*. John Wiley and Sons, New York, 2000.

[4] Ted Belytschko and Robert Mullen. Stability of explicit-implicit mesh partitions in time integration. *International Journal for Numerical Methods in Engineering*, **12**(10):1575–1586, 1978.

[5] E. J. Caramana, D. E. Burton, M. J. Shashkov, and P. P. Whalen. The construction of compatible hydrodynamics algorithms utilizing conservation of total energy. *Journal of Computational Physics*, **146**(1):227–262, October 1998.

[6] E. J. Caramana, C. L. Rousculp, and D. E. Burton. A compatible, energy and symmetry preserving lagrangian hydrodynamics algorithm in three-dimensional cartesian geometry. *Journal of Computational Physics*, **157**(1):89–119, January 2000.

[7] Andrew W. Cook and William H. Cabot. A high-wavenumber viscosity for high-resolution numerical methods. Technical Report UCRL-ID-152002, Lawrence Livermore National Laboratory, Livermore, CA, February 2003.

[8] Andrew W. Cook and William H. Cabot. A high-wavenumber viscosity for high-resolution numerical methods. *Journal of Computational Physics*, **195**(2):594–601, April 2004.

[9] Robert D. Cook, David S. Malkus, and Michael E. Plesha. *Concepts and Applications of Finite Element Analysis*. John Wiley & Sons, New York, 3rd edition, 1989.

[10] Alain Curnier. *Computational Methods in Solid Mechanics*. Kluwer Academic Publishers, May 1994.

[11] W. Dettmer and D. Peric. An analysis of the time integration algorithms for the finite element solutions of incompressible navier stokes equations based on a stabilised formulation. *Computer Methods in Applied Mechanics and Engineering*, **192**(9-10):1177–1226, February 2003.

[12] D. P. Flanagan and T. Belytschko. Eigenvalues and stable time steps for the uniform strain hexahedron and quadrilateral. *ASME Journal of Applied Mechanics*, **51**(1):35–40, 1984.

[13] Stephen H. Friedberg, Arnold J. Insel, and Lawrence E. Spence. *Linear Algebra*. Prentice Hall, fourth edition, November 2002.

[14] Amos Gilat. *MATLAB: An Introduction with Applications*. Wiley, 3rd edition, 2008.

[15] Brian Hahn and Dan Valentine. *Essential MATLAB for Engineers and Scientists*. Newnes, 3rd edition, March 2007.

[16] John O. Hallquist. LS-DYNA theory manual. Technical report, Livermore Software Technology Corporation, Livermore, CA, March 2006. (www.lstc.com).

[17] Thomas J. R. Hughes. Analysis of transient algorithms with particular reference to stability behavior. In Ted Belytschko and Thomas J. R. Hughes, editors, *Computational Methods for Transient Analysis*, chapter 2, pages 67–155. North-Holland, Amsterdam, January 1983.

[18] Thomas J. R. Hughes. *The Finite Element Method: Linear Static and Dynamic Finite Element Analysis*. Dover Publications, 2000.

[19] Gregory M. Hulbert and Jintai Chung. Explicit time integration algorithms for structural dynamics with optimal numerical dissipation. *Computer Methods in Applied Mechanics and Engineering*, **137**(2):175–188, October 1996.

[20] C. T. Kelley. *Iterative Methods for Linear and Nonlinear Equations*, volume 16 of *Frontiers in Applied Mathematics*. SIAM, Philadelphia, 1995.

[21] Steen Krenk. Dispersion-corrected explicit integration of the wave equation. *Computer Methods in Applied Mechanics and Engineering*, **191**(8-10):975–987, December 2001.

[22] Erwin Kreyszig. *Introductory Functional Analysis with Applications*, volume 17 of *Wiley Classics Library Series*. John Wiley & Sons, New York, 1989.

[23] Raymond D. Krieg and Samuel W. Key. Transient shell response by numerical time integration. *International Journal for Numerical Methods in Engineering*, **7**(3):273–286, 1973.

[24] Raphael Loubere and Mikhail J. Shashkov. A subcell remapping method on staggered polygonal grids for arbitrary-lagrangian eulerian methods. *Journal of Computational Physics*, **209**(1):105–138, October 2005.

[25] E. Love and M. K. Wong. Lagrangian continuum dynamics in Alegra. Technical Report SAND2007-8104, Sandia National Laboratories, Albuquerque, NM, December 2007.

[26] Ralph Menikoff and Bradley J. Plohr. The Riemann problem for fluid flow of real materials. *Reviews of Modern Physics*, **61**(1):75–130, January 1989.

[27] Robert Mullen and Ted Belytschko. Dispersion analysis of finite element semidiscretizations of the two-dimensional wave equation. *International Journal for Numerical Methods in Engineering*, **18**(1):11–29, January 1982.

[28] K. C. Park. Practical aspects of numerical time integration. *Computers & Structures*, **7**(3):343–353, June 1977.

[29] Richard B. Pember and Robert W. Anderson. Comparison of staggered-mesh lagrange plus remap and cell-centered direct eulerian godunov schemes for eulerian shock hydrodynamics. Technical Report UCRL-JC-139820, Lawrence Livermore National Laboratory, Livermore, CA, November 2000.

[30] Robert D. Richtmyer and K.W. Morton. *Difference Methods for Initial-Value Problems*. John Wiley & Sons, New York, second edition, 1967.

[31] Howard L. Schreyer. Dispersion of semidiscretized and fully discretized systems. In Ted Belytschko and Thomas J. R. Hughes, editors, *Computational Methods for Transient Analysis*, chapter 6, pages 267–299. North-Holland, Amsterdam, January 1983.

[32] G. Scovazzi, E. Love, and M. Shashkov. A multi-scale q1/p0 approach to langrangian shock hydrodynamics. Technical Report SAND2007-1423, Sandia National Laboratories, Albuquerque, NM, March 2007.

[33] G. Scovazzi, E. Love, and M. J. Shashkov. Multi-scale lagrangian shock hydrodynamics on q1/p0 finite elements: Theoretical framework and two-dimensional computations. *Computer Methods in Applied Mechanics and Engineering*, **197**(9-12):1056–1079, February 2008.

[34] Denis Serre. *Matrices: Theory and Applications*, volume 216 of *Graduate Texts in Mathematics*. Springer, New York, August 2002.

[35] J. C. Simo and N. Tarnow. The discrete energy-momentum method. Conserving algorithms for nonlinear elastodynamics. *Zeitschrift fur Angewandte Mathematik und Physik (ZAMP)*, **43**(5):757–792, September 1992.

[36] John C. Strikwerda. *Finite Difference Schemes and Partial Differential Equations*. Chapman & Hall, New York, 1989.

[37] Jeffrey W. Swegle. TOODY IV: a computer program for two dimensional wave propagation. Technical Report SAND78-0552, Sandia National Laboratories, Albuquerque, NM, September 1978.

[38] L. M. Taylor and D. P. Flanagan. Pronto 3d : A three-dimensional transient solid dynamics program. Technical Report SAND87-1912, Sandia National Laboratories, Albuquerque, NM, March 1989.

[39] Stephen Wolfram. *The Mathematica Book*. Cambridge University Press, 4th edition, March 1999.

[40] J. P. Woodruff. Kovec user's manual. Technical Report UCID-17306, Lawrence Livermore National Laboratory, Livermore, CA, November 1976.

[41] Paul Woodward and Phillip Colella. The numerical simulation of two-dimensional fluid flow with strong shocks. *Journal of Computational Physics*, **54**(1):115–173, April 1984.

DISTRIBUTION:

1 Andrew J. Barlow
Design Physics Department
AWE Aldermaston
Reading
Berkshire
RG7 4PR
United Kingdom

1 Alan S. Dawes
Computational Physics Group
AWE Aldermaston
Reading
Berkshire
RG7 4PR
United Kingdom

1 Robert Doney
US Army Research Laboratory
AMSRD-ARL-WM-TA
Aberdeen Proving Ground, MD 21005-5066

1 Brian Leavy
US Army Research Laboratory
AMSRD-ARL-WM-TA
Aberdeen Proving Ground, MD 21005-5066

1 Robert N. Rieben
Scientific B-Division
Lawrence Livermore National Laboratory
7000 East Ave., L-095
Livermore, CA 94551

1 Mikhail Shashkov
Theoretical Division, Group T-7
MS-B284
Los Alamos National Laboratory
Los Alamos, NM 87545

1 MS 1318
James R. Stewart, 1411

1 MS 0370
Timothy G. Trucano, 1411

1 MS 1320
S. Scott Collis, 1416

1 MS 0378
Randall M. Summers, 1431

1 MS 0378
Edward Love, 1431

1 MS 0378
William J. Rider, 1431

1 MS 0378
Allen C. Robinson, 1431

1 MS 1319
Guglielmo Scovazzi, 1431

1 MS 0378
O. Erik Strack, 1431

1 MS 0378
V. Gregory Weirs, 1431

1 MS 0378
Michael K. Wong, 1431

1 MS 0316
Curtis C. Ober, 1433

1 MS 0378
Thomas E. Voth, 1433

1 MS 1322
John B. Aidun, 1435

1 MS 1322
John H. Carpenter, 1435

1 MS 1322
Joshua Robbins, 1435

1 MS 0316
John N. Shadid, 1437

1 MS 0372
Arne S. Gullerud, 1524

1 MS 0836
David A. Crawford, 1541

1 MS 0380
Joseph Jung, 1542

1 MS 0380
Jason D. Hales, 1542

1 MS 0380
Martin Heinstein, 1542

1 MS 0380
Kendall H. Pierson, 1542

1 MS 0380
Benjamin W. Spencer, 1542

1 MS 1189
Thomas A. Brunner, 1641

1 MS 1186
Kyle R. Cochrane, 1641

1 MS 1186
Christopher J. Garasi, 1641

1 MS 1189
Thomas A. Gardiner, 1641

1 MS 1189
Thomas A. Haill, 1641

1 MS 1189
Heath L. Hanshaw, 1641

1 MS 0899
Technical Library, 9536 (electronic copy)